

**Analog and Mixed-Signal Products**

# **Analog Applications Journal**

**Fourth Quarter, 2003**



## IMPORTANT NOTICE

Texas Instruments Incorporated and its subsidiaries (TI) reserve the right to make corrections, modifications, enhancements, improvements, and other changes to its products and services at any time and to discontinue any product or service without notice. Customers should obtain the latest relevant information before placing orders and should verify that such information is current and complete. All products are sold subject to TI's terms and conditions of sale supplied at the time of order acknowledgment.

TI warrants performance of its hardware products to the specifications applicable at the time of sale in accordance with TI's standard warranty. Testing and other quality control techniques are used to the extent TI deems necessary to support this warranty. Except where mandated by government requirements, testing of all parameters of each product is not necessarily performed.

TI assumes no liability for applications assistance or customer product design. Customers are responsible for their products and applications using TI components. To minimize the risks associated with customer products and applications, customers should provide adequate design and operating safeguards.

TI does not warrant or represent that any license, either express or implied, is granted under any TI patent right, copyright, mask work right, or other TI intellectual property right relating to any combination, machine, or process in which TI products or services are used. Information published by TI regarding third-party products or services does not constitute a license from TI to use such products or services or a warranty or endorsement thereof. Use of such information may require a license from a third party under the patents or other intellectual property of the third party, or a license from TI under the patents or other intellectual property of TI.

Reproduction of information in TI data books or data sheets is permissible only if reproduction is without alteration and is accompanied by all associated warranties, conditions, limitations, and notices. Reproduction of this information with alteration is an unfair and deceptive business practice. TI is not responsible or liable for such altered documentation.

Resale of TI products or services with statements different from or beyond the parameters stated by TI for that product or service voids all express and any implied warranties for the associated TI product or service and is an unfair and deceptive business practice. TI is not responsible or liable for any such statements.

### Mailing Address:

Texas Instruments  
Post Office Box 655303  
Dallas, Texas 75265

Copyright © 2003, Texas Instruments Incorporated

# Contents

<b>Introduction</b> .....	4
<b>Data Acquisition</b>	
<b>ADS82x ADC with non-uniform sampling clock</b> .....	5
A growing number of applications require ADCs to operate from a sampling clock with variable frequency, phase, or duty cycle. This article shows that TI's ADS82x can operate very well with a non-uniform sampling clock.	
<b>Calculating noise figure and third-order intercept in ADCs</b> .....	11
Noise figure (NF) and third-order intercept point ( $IP_3$ ) are not common specifications for analog-to-digital converters (ADCs). This article shows how to calculate NF and $IP_3$ in ADCs by using known specifications for the signal-to-noise ratio; the two-tone, third-order intermodulation distortion ( $IMD_3$ ); and the signal level at the input.	
<b>Evaluation criteria for ADSL analog front end.</b> .....	16
This article describes several important ADSL analog front end evaluation criteria and design limitation factors, including the relationship between total signal-to-noise ratio and transmission data speed; loop attenuation variation with discrete multitone signal frequency and its influence on the reach; the echo return loss of the hybrid circuit; and the impact of the multitone power ratio.	
<b>Power Management</b>	
<b>UCC28517 100-W PFC power converter with 12-V, 8-W bias supply, Part 2.</b> .....	21
To conclude the review of the UCC28517 PFC supply, this article covers the design of the second 12-V, 8-W power stage to be used as an auxiliary bias supply.	
<b>Amplifiers: Op Amps</b>	
<b>Calculating noise figure in op amps</b> .....	28
Noise figure traditionally has not been used as a specification for op amps. Manufacturers long ago adopted input-referred voltage and current noise. This article shows how to calculate noise figure in op amps by using the circuit configuration and input-referred noise specifications. The calculations are detailed for inverting and non-inverting single-ended op amp amplifiers and for fully differential op amp amplifiers.	
<b>Index of Articles</b> .....	35
<b>TI Worldwide Technical Support</b> .....	38

**To view past issues of the**  
***Analog Applications Journal*, visit the Web site**  
**[www.ti.com/sc/analogapps](http://www.ti.com/sc/analogapps)**

# Introduction

*Analog Applications Journal* is a collection of analog application articles designed to give readers a basic understanding of TI products and to provide simple but practical examples for typical applications. Written not only for design engineers but also for engineering managers, technicians, system designers and marketing and sales personnel, the book emphasizes general application concepts over lengthy mathematical analyses.

These applications are not intended as “how-to” instructions for specific circuits but as examples of how devices could be used to solve specific design requirements. Readers will find tutorial information as well as practical engineering solutions on components from the following categories:

- Data Acquisition
- Power Management
- Amplifiers: Op Amps

Where applicable, readers will also find software routines and program structures. Finally, *Analog Applications Journal* includes helpful hints and rules of thumb to guide readers in preparing for their design.

# ADS82x ADC with non-uniform sampling clock

By Hui-Qing Liu (Email: liu\_hui-qing@ti.com)

Applications Engineer, High-Speed Products

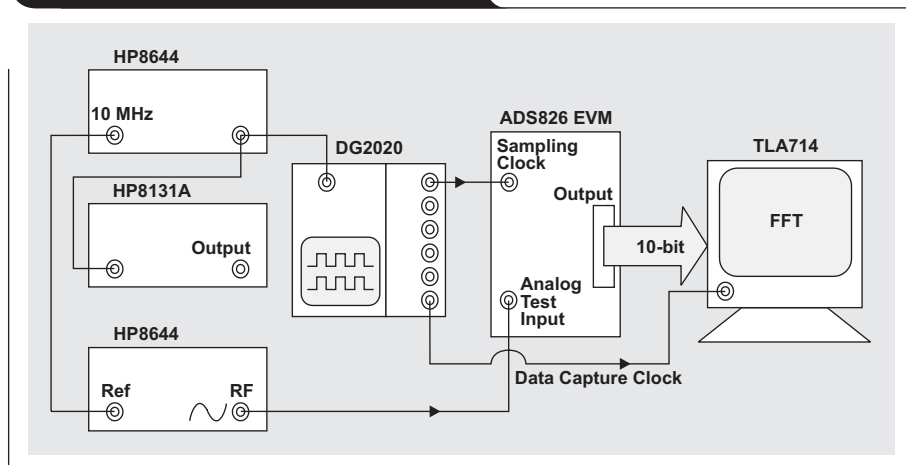
## Introduction

The Texas Instruments (TI) high-speed analog-to-digital converter (ADC) ADS82x family includes ADS825/822, ADS826/823, and ADS828. These ADCs have 10-bit resolution with a maximum sampling speed of 40, 60, and 75 MHz, respectively. They are widely used in communications, video digitizing, test equipment, CCD imaging, and medical ultrasound imaging. In some applications the ADCs are driven by a continuous sampling clock with constant frequency. However, in other applications such as medical ultrasound imaging or where the ADCs are parallel with interleaved configuration, they must operate with a sampling clock that

has variable frequency, phase, or duty cycle. In other words, these ADCs must operate with a non-uniform sampling clock. Can TI's ADS82x handle this? A lab bench test has shown good results, and the answer is *yes*. This article presents the measurement system and fast Fourier transform (FFT) analysis method used along with the test results for only the ADS826 EVM. However, these test results are applicable to all other ADCs in the ADS82x family, since these ADCs all have pipeline architecture and are designed with the same basic features, such as 10-bit resolution, internal or external reference, single-ended or differential analog input, input range selection, single 5-V

power supply, power-down mode, low power dissipation, three-state output, and CMOS- or TTL-output compatibility.

Figure 1. ADS82x bench test system



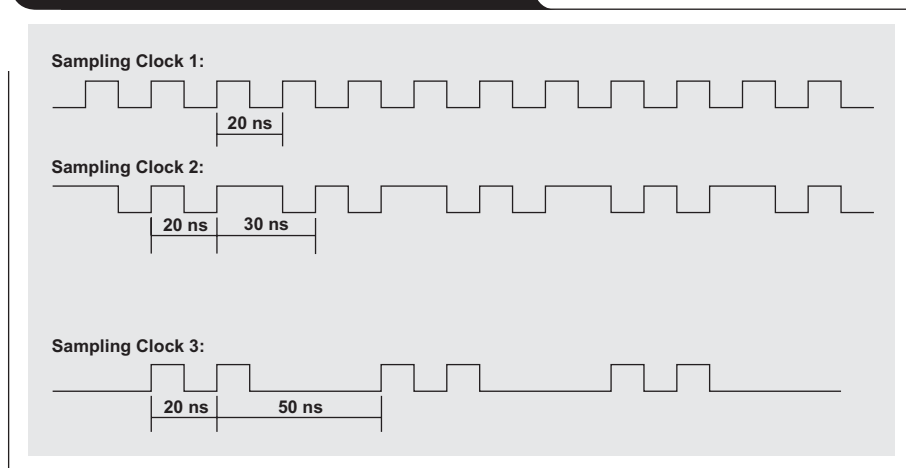
## Test system

The ADS826 bench test system includes a pulse generator (HP8131A), data generator (DG2020), waveform generator (HP8644), and Tektronix logic analyzer (TLA714) (see Figure 1). This system is used to generate an analog signal, pattern clock, and data capture clock. The analog signal, a sine wave that can be varied in frequency and amplitude, is an input test signal to the ADS826; and the pattern clock, which can be varied in frequency, phase, or duty cycle, is the sampling clock to the ADS826. The data capture clock can be flexible with a proper frequency and duty cycle for the TLA714 to capture data from the ADS826 EVM and perform FFT analysis. The clock source is phase locked with the test signal source by the 10-MHz reference output of the HP8644, so all the signals generated from the system are synchronized. The HP8131A is used to calibrate DG2020.

## Pattern clocks

Three different pattern clocks, plotted in Figure 2, are generated from this system. They are used to test the non-uniform sampling performance of

Figure 2. Pattern clocks for ADS826 test



the ADS826. Sampling Clock 1 (Case 1) is a uniform clock with a frequency of 50 MHz and a duty cycle of 50%. Sampling Clock 2 (Case 2) is a non-uniform clock with frequency (varied cycle by cycle) alternating from 50 MHz with a 50% duty cycle to 33.3 MHz with a 66.7% duty cycle. Sampling Clock 3 (Case 3) is a non-uniform clock with frequency varying (cycle by cycle) from 50 MHz with a 50% duty cycle to 20 MHz with a 20% duty cycle. These clocks are simulated from real applications.

### ADS826 input/output configuration

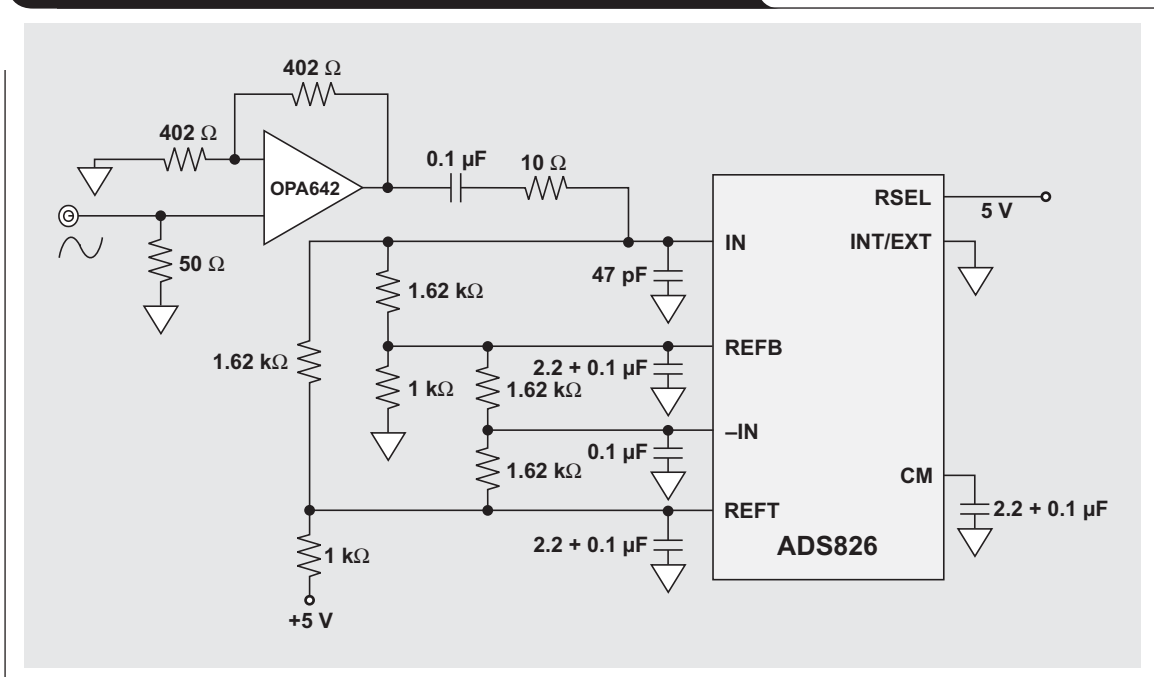
The single-ended analog input circuit used in this test is shown in Figure 3. Here an OPA642 with an inverting gain of 2 is used. This circuit mainly provides two conditions for the ADS826. One is an ac-coupled signal path with a power amplifier with proper gain and driving capability; another is the common-mode dc voltage for the ADS826 analog input bias. The ADS826 is configured with an internal reference and a full-scale input range of  $2V_{p-p}$ . The common-mode pin (CM) is not used here except for bypassing. Based on the configuration, a  $2V_{p-p}$  analog sine wave is applied to +IN, and a 2.35-V common-mode dc voltage is added to both +IN and -IN of the ADS826 analog input. This common-mode voltage is generated by REFT, REFB, and an external 5-V power supply through a balanced resistor network. The input clock of ADS826 from DG2020 is one of the three sampling clocks mentioned earlier. The digital output of the ADS826 is connected to the TLA714 through a data bus driver such as TI's SN74x family. The digital configuration of ADS826 is straightforward and is therefore not shown in Figure 3. Details about the ADS826 digital output circuit can be found in Reference 1.

### Data measurement and analysis

A TLA714 is used to collect the output data from the ADS826, and the performance of the device is evaluated using FFT analysis. For this approach, the sampling clock of the ADS826 and the input clock of the TLA714 need to be synchronized with the analog input test signal. When the signal is synchronized, the data is ready to be measured. In the beginning, the analog sine wave is sampled by the ADS826 at the rising edge of the sampling clock, and the sample is converted into digital form in the pipeline stage. Five sampling clocks later, a digital number (straight offset binary code) of the sample is output to the data bus of the ADS826 with additional small-signal propagation. The digital data is sent to the data bus by the ADS826 at the rising edge of the input sampling clock. It stays on the bus for one clock period and is then updated at the next rising edge of the input sampling clock by new sample data. When the data is valid on the data bus, it is captured by the logic analyzer with a synchronized clock. The data is then processed and analyzed using FFT analysis.

The three different sampling cases mentioned earlier are evaluated here. In Case 1 the sampling clock frequency of ADS826 is constant at 50 MHz; in Case 2 the sampling clock frequency of ADS826 is not constant and is regularly varied 20 ns or 30 ns on a cycle-by-cycle basis; and in Case 3 the sampling clock period of the ADS826 is regularly varied by 20 ns or 50 ns. Sampling Clocks 2 and 3 are non-uniform sampling clocks, and their phases change with time. This is clearly demonstrated by Sampling Clock 3, where the clock phase is delayed for 30 ns after each two 50-MHz clock cycles. Such sampling phase variation is apparent

**Figure 3. Single-ended input circuit for ADS826 bench test**



from the output data of the ADS826. In Case 1, the ADS826 samples the analog sine wave and constantly outputs the digitized samples at 50 MSPS. In Cases 2 and 3, the analog sine wave is sampled by the ADS826 at variable speed so that the digitized samples are sent out in non-uniform time intervals. This is shown in Figures 4–6. Further analysis of the non-uniform sampling performance of the ADS826 is presented later under “Test results.”

Does the ADS826 operate as well with a non-uniform sampling clock as it

**Figure 4. Non-uniform sampling time intervals**

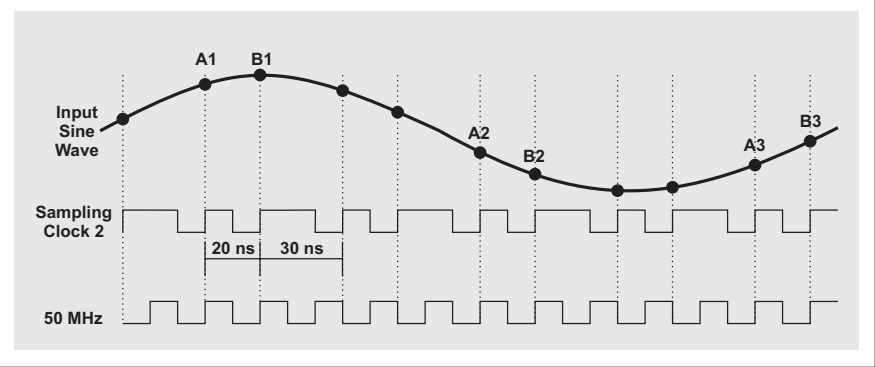


**Figure 5. ADS826 non-uniform sampling performance analysis for Case 2**

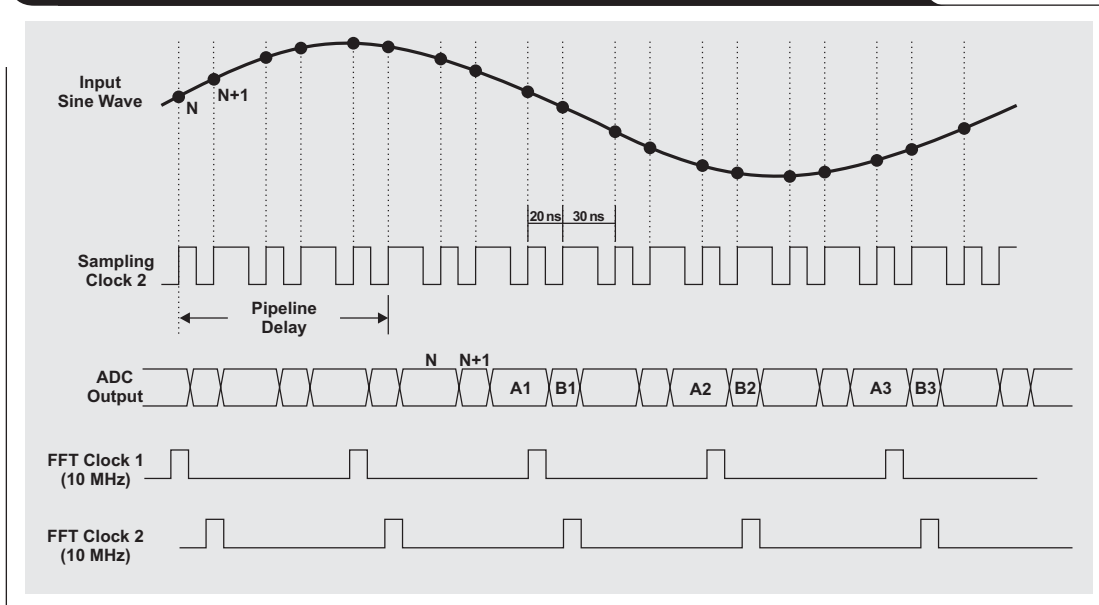
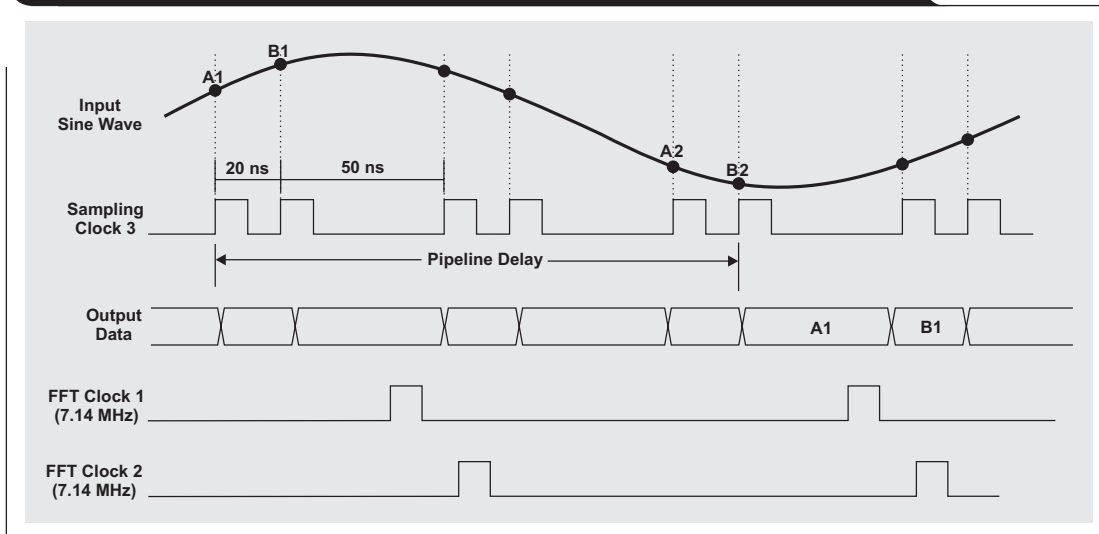


**Figure 6. ADS826 non-uniform sampling performance analysis for Case 3**



does with a uniform sampling clock? Yes, and this can be explained by the downsampling technique and the FFT analysis. In FFT analysis, the sample size is kept at 4096; and the FFT sampling frequency is kept more than five times higher than the signal frequency for all three cases. In Case 1 with Sampling Clock 1, the output data of the ADS826 can be used directly as the FFT input because of the uniform samples; and the FFT result is the specification in the data sheet. In Cases 2 and 3 with a non-uniform sampling clock, the output data of the ADS826 cannot be used directly as the FFT input due to non-uniform samples. To perform the FFT analysis for Cases 2 and 3, we need to find a set of uniform samples from non-uniform ADC sampling data. The implementation of this idea is shown in Figure 4, where the ADS826 samples an analog sine wave at the rising edge of Sampling Clock 2 and the sample locations on the sine wave have non-uniform time intervals. With FFT downsampling techniques, however, these locations can be classified into uniform time-interval sets. For example, by using a 50-MHz clock as a uniform time reference, we can find data set A (A1, A2, A3...) and data set B (B1, B2, B3...) in which the data is uniformly spaced. Furthermore, data set A results from fast-sampling Clock 2 (50 MHz), and data set B results from slow-sampling Clock 2 (33.3 MHz). The data in each set is uniformly time-spaced by the 10-MSPS FFT sampling frequency, which downsamples the original data. This frequency can

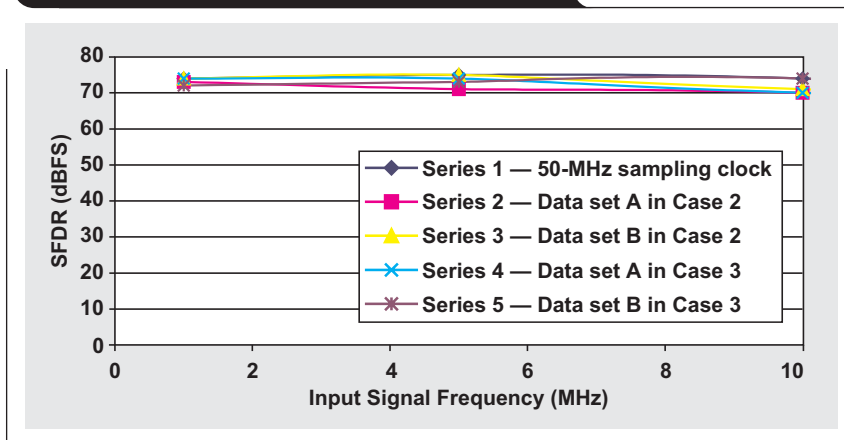
be used as a clock frequency of the logic analyzer that is used to extract data set A or B from the data bus of the ADS826.

The completed data acquisition from the ADS826 with a non-uniform sampling clock is shown in Figure 5, where sample N on the sine wave is collected by the ADS826 at the rising edge of the input clock and is output after a period of five input clocks. The input clock consists of fast and slow clocks, while the ADS826 output data consists of long and short periods. Because of the five-clock delay, sample N from the fast input clock appears on the output data bus for a long period, and sample N+1 from the slow input clock appears on the output data bus for a short period. For FFT analysis, FFT Clock 1 (10 MHz) is used to capture data set A, while FFT Clock 2 (10 MHz with a 20-ns clock delay) is used to capture data set B. The output results of data sets A and B represent the dynamic performance of the ADS826 with non-uniform Sampling Clock 2, as shown later under "Test results."

The same principle is applied in Case 3, which is shown in Figure 6. In this case the frequency of FFT Clocks 1 and 2 is 7.14 MHz. With a different sampling clock pattern, the downsampling clock frequency for FFT will vary and may be difficult to determine. The test results show that the ADS826 functions well with a non-uniform sampling clock as long as the clock high and low pulse width is at least half the period of the highest sampling clock specified in the data sheet; for example, a pulse width of at least 8.3 ns for the ADS826

(maximum speed is 60 MHz). The sampling clock speed also has to meet the minimum limit in the data sheet.

**Figure 7. SFDR of ADS826 with uniform and non-uniform sampling clocks**



## Test results

Input analog signal frequencies of up to 30 MHz for all three cases were tested, and the results are shown in Table 1 and Figure 7. Table 1 shows that there is no change in the signal-to-noise ratio (SNR) whether the ADS826 is driven by a uniform or non-uniform sampling clock. Figure 7 shows that there is also no significant difference in spurious-free dynamic range (SFDR) performance between uniform and non-uniform sampling. In addition, for

**Table 1. SNR (dBFS) of ADS826**

	SAMPLING CLOCK (MHz)	FFT CLOCK (MHz)	SNR (dBFS)			
			1-MHz Signal Frequency	5-MHz Signal Frequency	10-MHz Signal Frequency	30-MHz Signal Frequency
Case 1	50 (uniform)	50	60	60	60	58
Case 2	50 and 33.3 mixed (non-uniform)	10 (FFT Clock 1)	60	60	60	58
	50 and 33.3 mixed (non-uniform)	10 (FFT Clock 2)	60	60	60	58
Case 3	50 and 20 mixed (non-uniform)	7.14 (FFT Clock 1)	60	60	60	58
	50 and 20 mixed (non-uniform)	7.14 (FFT Clock 2)	60	60	60	58

non-uniform sampling, the SFDR increases when the sampling clock or input signal amplitude decreases.

The FFT test result is shown in Figures 8–10. Figure 8 shows the FFT output of Case 1 and the performance of ADS826 with a 50-MHz sampling clock and a 1-MHz input sine wave at maximum amplitude. The SNR is 60 dBFS, and the SFDR is 74 dBFS. The FFT output of Case 2 is shown in Figure 9, in which the non-uniform ADC samples are downsampled by a 10-MHz FFT clock. Figure 9a shows the FFT output of data set A, and Figure 9b shows the FFT output of data set B. The SNR is 60 dBFS for both data sets A and B; the SFDR is 73 dBFS for data set A and 74 dBFS for data set B. The FFT output of Case 3 is shown in Figure 10, in which the non-uniform ADC samples are downsampled by a 7.143-MHz FFT clock. The SNR is 60 dBFS for both data sets A and B; the SFDR is 74 dBFS for data set A and 72 dBFS for data set B.

## Conclusion

The test results presented in this article strongly support non-uniform sampling applications of the ADS82x family. The test results show that the same SNR is achieved with both uniform and non-uniform sampling using the ADS826. Good SFDR is also achieved with both uniform and non-uniform sampling. The test data and analysis conclude that the ADS826 functions well with a non-uniform sampling clock as long as the clock high and low pulse width is at least half the period of the highest sampling clock specified in the data sheet. The test result proves that the ADS82x family has a very stable and solid SNR of 10 bits of resolution in both uniform and non-uniform high-speed sampling and converting operations, making it appropriate for wide use in future applications.

**Figure 8. FFT output with 50-MHz uniform sampling (Case 1)**

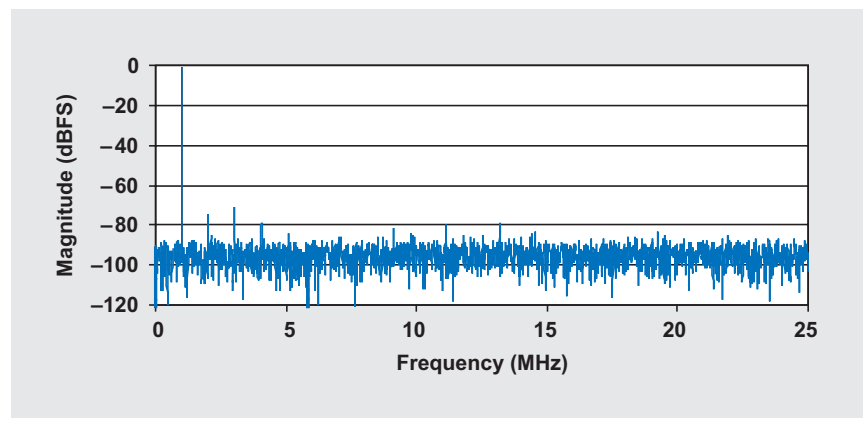


**Figure 9. Case 2 FFT outputs with 10-MHz downsampling frequency**

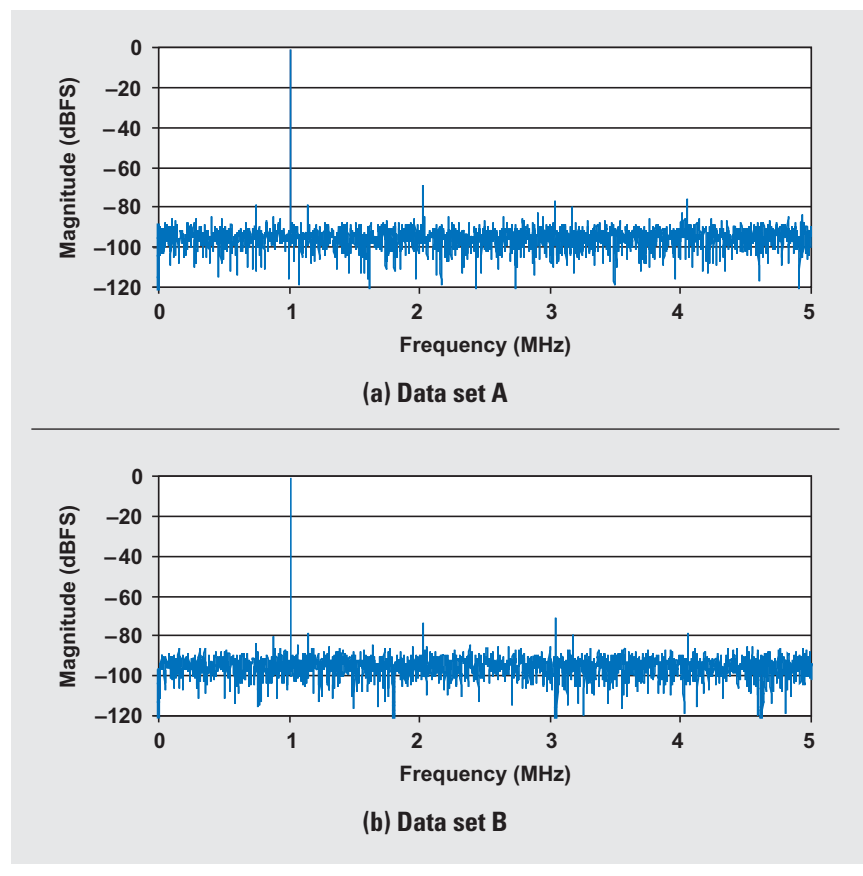
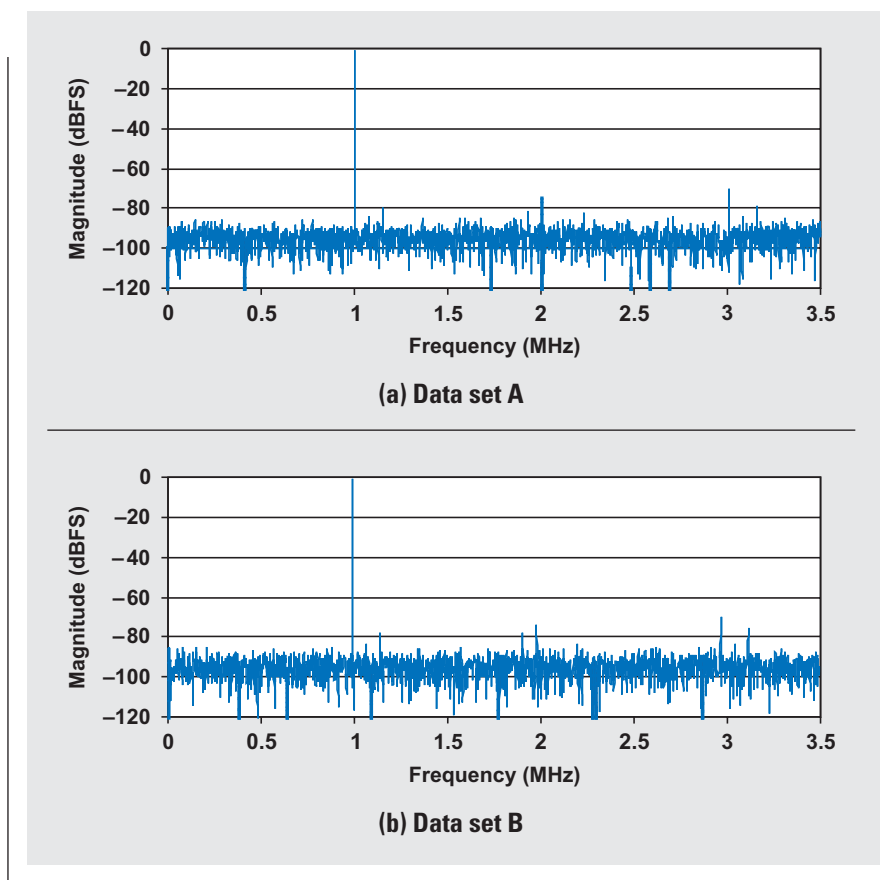


**Figure 10. Case 3 FFT outputs with 7.14-MHz downsampling frequency**



**References**

For more information related to this article, you can download an Acrobat Reader file at [www-s.ti.com/sc/techlit/litnumber](http://www-s.ti.com/sc/techlit/litnumber) and replace “*litnumber*” with the **TI Lit. #** for the materials listed below.

Document Title	TI Lit. #
1. “DEM-ADS82xE Evaluation Fixture,” User Guide .....	.sbau036
2. “10-Bit, 60MHz Sampling Analog-to-Digital Converter,” Data Sheet .....	.sbas070
3. Alan V. Oppenheim and Ronald W. Schaffer, <i>Discrete-Time Signal Processing</i> (Prentice-Hall, Inc., 1989).	—

**Acknowledgments**

Special thanks go to Bryan McKay and Rosie Loaiza for their support on the test board and to Stephan Baier for his article review.

**Related Web sites**

[analog.ti.com](http://analog.ti.com)  
[www.ti.com/sc/device/partnumber](http://www.ti.com/sc/device/partnumber)  
 Replace *partnumber* with ADS822, ADS823, ADS825, ADS826, ADS828 or OPA642

# Calculating noise figure and third-order intercept in ADCs

By James Karki (Email: j-karki@ti.com)

Member, Group Technical Staff, High-Performance Linear

## Introduction

Noise figure (NF) and the third-order intercept point ( $IP_3$ ) are used in radio receiver link budget analysis as a means to quantify the effects of device noise and nonlinearity on the sensitivity of the radio. Analog-to-digital converters (ADCs) are used in radio receivers to convert the signal from the analog domain to the digital domain. NF and  $IP_3$  typically are not specified for the device, but equivalent parameters are given whereby they can be calculated.

ADCs specify signal-to-noise ratio (SNR) and two-tone, third-order intermodulation distortion ( $IMD_3$ ) under certain input signal and clocking conditions. With this information, NF and  $IP_3$  can be calculated.

In general, a low NF and high  $IP_3$  are desired. The actual values required to meet the design goals depend on the architecture of the system.

## Review of noise figure

Noise figure (NF) is the decibel equivalent of noise factor (F):  $NF \text{ (dB)} = 10\log(F)$ .

Noise factor of a device is the power ratio of the SNR at the input ( $SNR_I$ ) divided by the SNR at the output ( $SNR_O$ ):

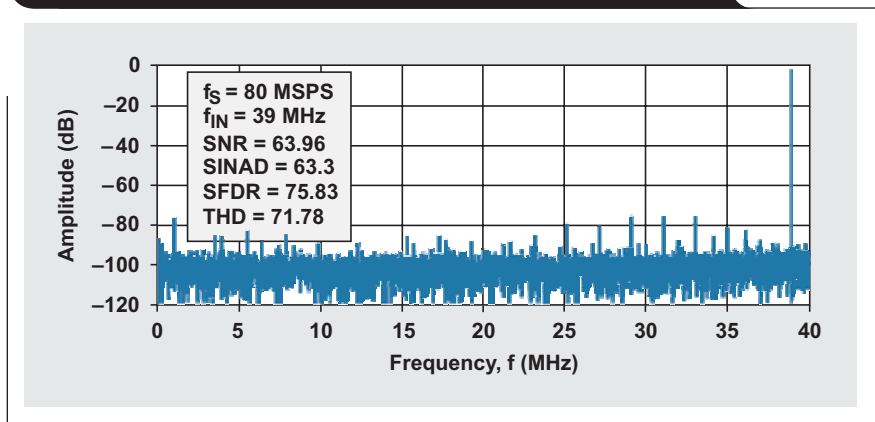
$$F = \frac{SNR_I}{SNR_O} \quad (1)$$

The output signal ( $S_O$ ) is equal to the input signal ( $S_I$ ) times the gain:  $S_O = S_I \times G$ . The output noise is equal to the noise delivered to the input ( $N_I$ ) from the source plus the input noise of the device ( $N_A$ ) times the gain:  $N_O = (N_I + N_A) \times G$ . Substituting into Equation 1 and simplifying, we get

$$F = \frac{SNR_I}{SNR_O} = \left[ \frac{\frac{S_I}{N_I}}{\frac{G \times S_I}{G \times (N_I + N_A)}} \right] = 1 + \frac{N_A}{N_I} \quad (2)$$

Assuming that the input is terminated in the same impedance as the source,  $N_I = kT = -174 \text{ dBm/Hz}$ , where  $k$  is Boltzman's constant and  $T = 300 \text{ Kelvin}$ ). Once we find the input noise spectral density of the device, it is a simple matter to plug it into Equation 2 and calculate F.

Figure 1. ADS5410 FFT or spectral plot from Reference 1



## NF in ADCs

There are a couple of ways to go about calculating the input noise spectral density of an ADC, but using the SNR specification is easy.

To measure SNR, a low-noise signal is input to the ADC, and the output is examined by taking a fast Fourier transform (FFT) or spectral plot. Figure 1 shows such a plot from Reference 1. The ratio of the signal to the noise integrated over half the sampling frequency ( $f_s/2$ ) is the SNR. Since the noise of the ADC is—to first-order approximation—independent of signal level, the higher the input level the better the SNR, up to a point. As the signal approaches full scale (FS), spurious behavior begins to degrade the SNR. An input signal level 1 dB below full-scale input ( $-1 \text{ dBFS}$ ) seems to give good results and is commonly used.

To find the input noise spectral density, we divide the signal level by the SNR divided by half the sampling frequency (since SNR is calculated by dividing the signal by the noise integrated over  $f_s/2$ ):

$$N_A \text{ (dBm/Hz)} = -1 \text{ dBFS (dBm)} + SNR \text{ (dBc)} - f_s/2 \text{ (dBHz)}$$

An ADC is a voltage-driven device, so we must choose an input resistance to find the signal power with the formula  $P = V^2/R$ . Assuming that  $FS = 2V_{p-p}$  and  $R = 50 \Omega$ , the full-scale input is  $+10 \text{ dBm}$ .

As an example of how to calculate, consider the following for the ADS5410, a 12-bit ADC. Given that  $f_s = 80 \text{ MSPS}$ ,  $R_{IN} = 50 \Omega$ ,  $FS = 2V_{p-p}$ , and  $SNR = 63.96$ , then

$$N_A \text{ (dBm/Hz)} = +9 \text{ dBm} - 63.96 \text{ dBc} - 76.02 \text{ dBHz} \\ = -130.98 \text{ dBm/Hz}$$

To use Equation 2, we need to use the linear equivalents of  $N_I$  and  $N_A$ :

$$F = 1 + 10E \left( \frac{-130.98 + 174}{10} \right) = 20045,$$

or  $NF \text{ (dB)} = 43.02 \text{ dB}$ .

Looking at the result, we see that adding the 1 in Equation 2 makes very little difference since the noise figure is so high. Therefore, using

$$NF \text{ (dB)} = N_A \text{ (dBm/Hz)} - N_I \text{ (dBm/Hz)}$$

introduces little error.

It is common practice to use a transformer or a fully differential op amp to drive high-performance ADCs differentially. This gives us the opportunity to use higher ADC input resistance. If  $NF$  is calculated based on  $50 \Omega$ , it is reduced by  $\log_{10}(\text{impedance ratio})$ .

For example, if we use a 1:4 impedance ratio (1:2 turns ratio) transformer, the input resistance is  $200 \Omega$  to match to a  $50\text{-}\Omega$  drive amplifier. The  $NF$  is reduced by  $10 \times \log_{10}(200/50) = 6 \text{ dB}$ . Or, if we use a 1:16 impedance ratio transformer with  $800\text{-}\Omega$  input resistance,  $NF$  is 12 dB lower.

### Review of third-order intercept point (IP<sub>3</sub>)

Due to nonlinearity in the transfer function of all electronics, distortion is generated. With reference to the formula of a straight line,  $y = b + mx$ , nonlinearity is any deviation

that the output ( $y$ ) may have from a constant multiple ( $m$ ) of the input ( $x$ ) plus any constant offset ( $b$ ).

Expanding the nonlinear transfer functions of basic transistor circuits into a power series is a typical way to quantify distortion products (see Reference 2). For example, transistors typically have an exponential transfer function (i.e., collector current vs. base emitter voltage),  $y = e^x$ , where  $x$  is the input and  $y$  is the output. Expanding  $e^x$  into a power series around  $x = 0$  results in

$$e^x = 1 + x + \frac{x^2}{2} + \frac{x^3}{6} + \frac{x^4}{24} + \frac{x^5}{120} + \dots + \frac{x^n}{n!}.$$

Figure 2 shows the function  $y = e^x$  along with estimates that use progressively more terms of the power series.

The farther  $x$  is from 0, the more terms are required to estimate the value of  $e^x$  properly. If  $x < 0.25$ , the linear term  $1 + x$  provides a close estimate of the actual function, and the circuit is linear. As  $x$  becomes larger, progressively more terms (quadratic, cubic, and higher-order distortion terms) are required to estimate  $e^x$  properly.

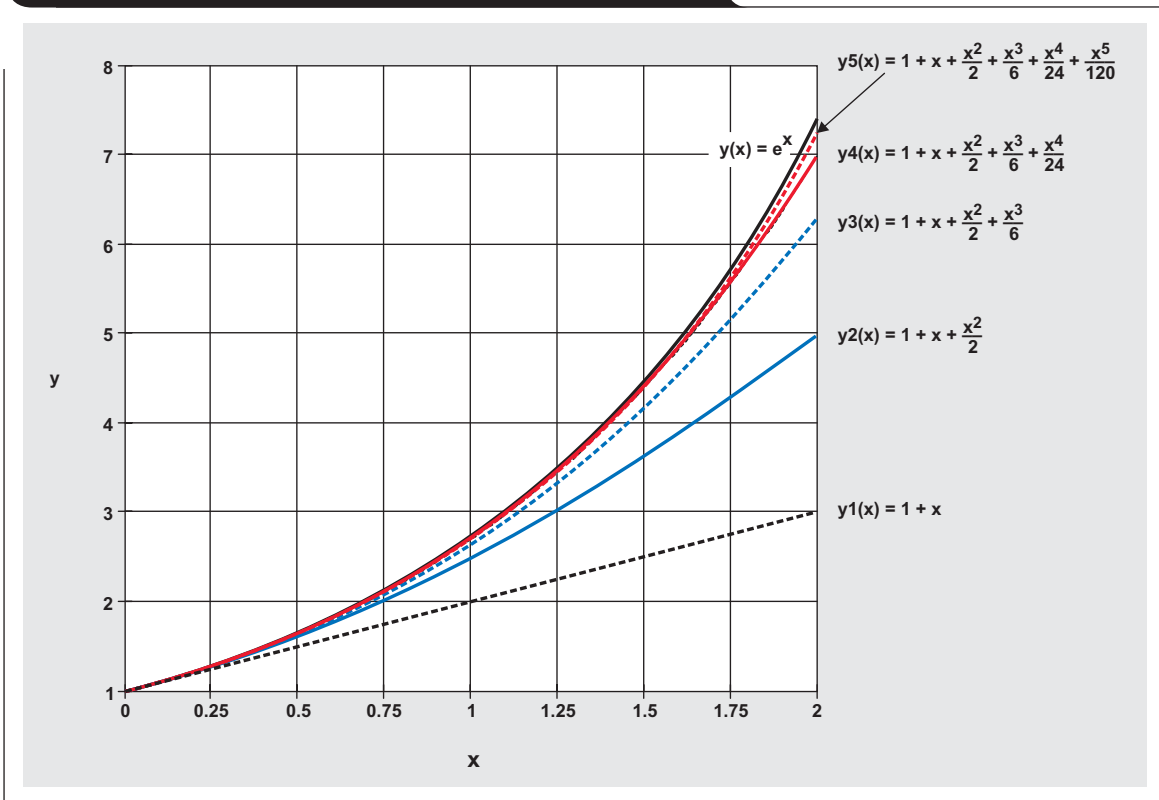
If the input to this circuit is a sinusoid—i.e.,  $x = A\sin(\omega t)$ —then the output

$$y = K_0 + K_1 A\sin(\omega t) + K_2 A^2 \sin^2(\omega t) + K_3 A^3 \sin^3(\omega t) + \dots,$$

where  $K_0, K_1$ , etc. are constant scaling factors. Using the trigonometric identities

$$\sin^2(\omega t) = \frac{1 - \cos(2\omega t)}{2} \text{ and}$$

**Figure 2. Function  $y = e^x$  and its power series estimates**



$$\sin^3(\omega t) = \frac{3\sin(\omega t) - \sin(3\omega t)}{4}$$

shows that the quadratic and cubic terms give rise to second- and third-order harmonic distortion (HD<sub>2</sub> and HD<sub>3</sub>, respectively). Similarly, higher-order terms give rise to higher-order harmonic distortion.

If the input is comprised of two tones—i.e.,  $x = A_1\sin(\omega_1 t) + A_2\sin(\omega_2 t)$ —then the output

$$y = K_0 + K_1[A_1\sin(\omega_1 t) + A_2\sin(\omega_2 t)] + K_2[A_1\sin(\omega_1 t) + A_2\sin(\omega_2 t)]^2 + K_3[A_1\sin(\omega_1 t) + A_2\sin(\omega_2 t)]^3 + \dots$$

where  $K_0, K_1$ , etc. are constant scaling factors.

Expanding the third term, we get

$$K_2[A_1\sin(\omega_1 t) + A_2\sin(\omega_2 t)]^2 = K_2[A_1^2\sin^2(\omega_1 t) + 2A_1A_2\sin(\omega_1 t)\sin(\omega_2 t) + A_2^2\sin^2(\omega_2 t)].$$

Using the trigonometric identities

$$\sin^2(\omega t) = \frac{1 - \cos(2\omega t)}{2} \text{ and}$$

$$\sin(\omega_1 t)\sin(\omega_2 t) = \frac{\cos(\omega_1 t - \omega_2 t) - \cos(\omega_1 t + \omega_2 t)}{2}$$

shows that the quadratic terms give rise to HD<sub>2</sub> and second-order intermodulation distortion (IMD<sub>2</sub>).

Expanding the fourth term, we get

$$K_3[A_1\sin(\omega_1 t) + A_2\sin(\omega_2 t)]^3 = K_3[A_1^3\sin^3(\omega_1 t) + 3A_1A_2\sin^2(\omega_1 t)\sin(\omega_2 t) + 3A_1A_2\sin(\omega_1 t)\sin^2(\omega_2 t) + A_2^3\sin^3(\omega_2 t)].$$

Using the trigonometric identities

$$\sin^3(\omega t) = \frac{3\sin(\omega t) - \sin(3\omega t)}{4} \text{ and}$$

$$\sin^2(\omega_1 t)\sin(\omega_2 t) = \frac{2\sin(\omega_2 t) - \sin(2\omega_1 t + \omega_2 t) - \sin(2\omega_2 t + \omega_1 t)}{4}$$

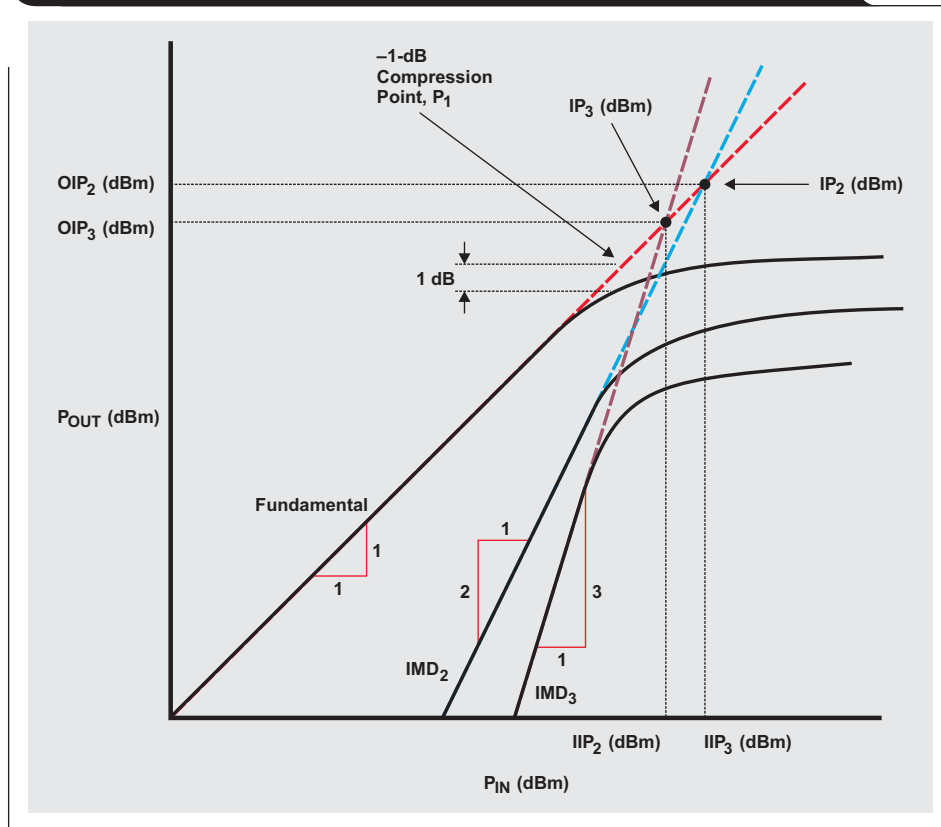
shows that the cubic terms give rise to HD<sub>3</sub> and third-order intermodulation distortion (IMD<sub>3</sub>). Similarly, higher-order terms give rise to higher-order harmonic and intermodulation distortion.

Table 1 shows the frequencies of the distortion products that will be generated due to second- and third-order nonlinearity, given a two-tone input at frequencies  $f_1$  and  $f_2$ .

**Table 1. Distortion product frequencies due to second- and third-order nonlinearity**

SECOND-ORDER FREQUENCIES		THIRD-ORDER FREQUENCIES	
$2f_1$	$2f_2$	$3f_1$	$3f_2$
$f_1 - f_2$	$f_1 + f_2$	$2f_1 - f_2$	$2f_2 - f_1$
		$2f_1 + f_2$	$2f_2 + f_1$

**Figure 3. Input and output two-tone and intermodulation distortion**



So now the question arises: Why is all this important? The answer is that radio specifications for GSM, CDMA2000, WCDMA, and the like all call for sensitivity requirements to be met with two interfering signals spaced in the frequency domain such that their third-order intermodulation product will fall on top of the signal of interest. The third-order intermodulation point is used to quantify how much distortion is generated. Referring this to the antenna input provides an easy method to determine whether or not the spec can be met.

If the input and output power of two tones applied to a device and their intermodulation products are graphed on a log-log scale as shown in Figure 3, the fundamental tones have a slope of 1, the second-order product has a slope of 2, and the third-order products have a slope of 3. The

device will go into compression before the lines intersect. The point where the output power is reduced by 1 dB from what is expected is called the 1-dB compression point ( $P_1$ ). By extending the lines, the second- and third-order intercept points ( $IP_2$  and  $IP_3$ , respectively) can be found. If they are referred to the input, they are called input intercept points ( $IIP_2$ ,  $IIP_3$ ); and if they are referred to the output, they are called output intercept points ( $OIP_2$ ,  $OIP_3$ ).

Since we are interested in intermodulation distortion relative to the carriers, why should we concern ourselves with some fictitious point that the amplifier will never reach? The answer is that there is a mathematical relationship between the two. Given the intercept point, we can calculate the intermodulation product for any input/output power.

Given that the slopes are known, equations for slopes  $L_1$  and  $L_3$  are written as shown in Figure 4.

Subtracting two arbitrary points on each line and rearranging gives us

$$y_2 - y_3 = x_2 - x_3 \Rightarrow y_2 = y_3 + x_2 - x_3 \text{ for } L1, \text{ and}$$

$$y_1 - y_3 = 3x_2 - 3x_3 \Rightarrow y_1 = y_3 + 3x_2 - 3x_3 \text{ for } L3.$$

Subtracting again results in

$$y_2 = y_3 + x_2 - x_3$$

$$-(y_1 = y_3 + 3x_2 - 3x_3)$$

$$\hline y_2 - y_1 = 2(x_3 - x_2).$$

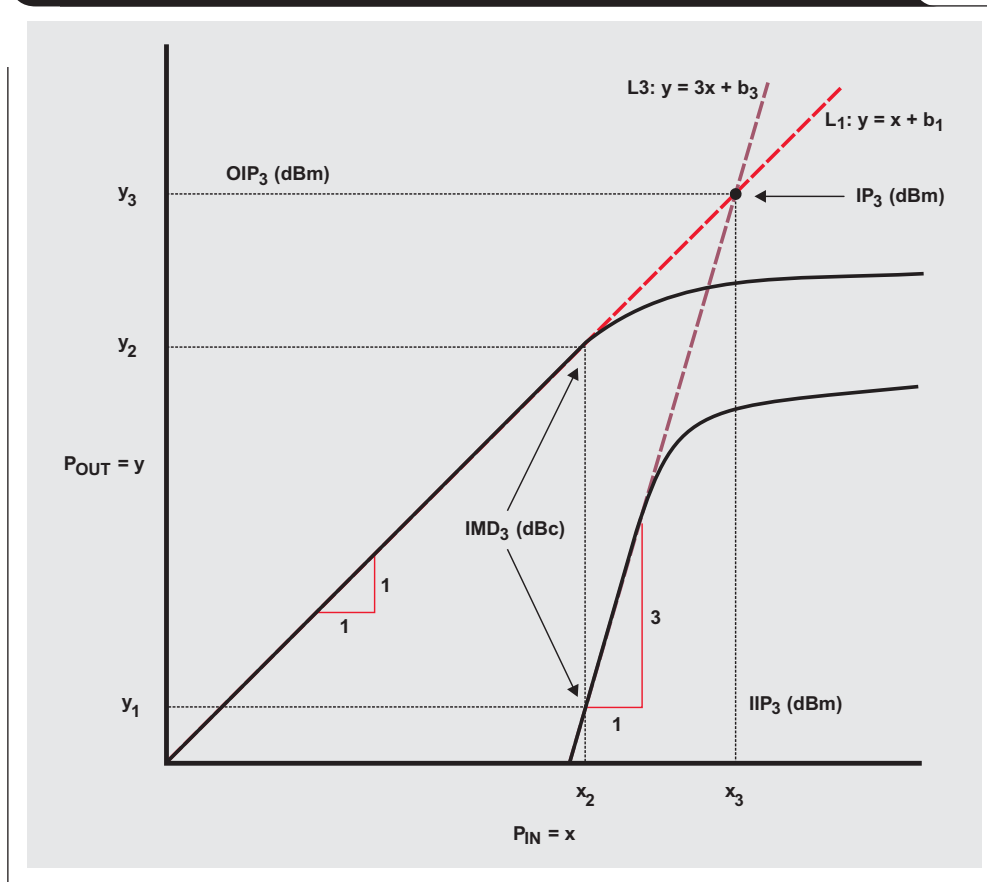
$\uparrow$   $\uparrow$   $\nwarrow$   
 $IMD_3 \text{ (dBc)}$   $IIP_3 \text{ (dBm)}$   $P_{IN}$

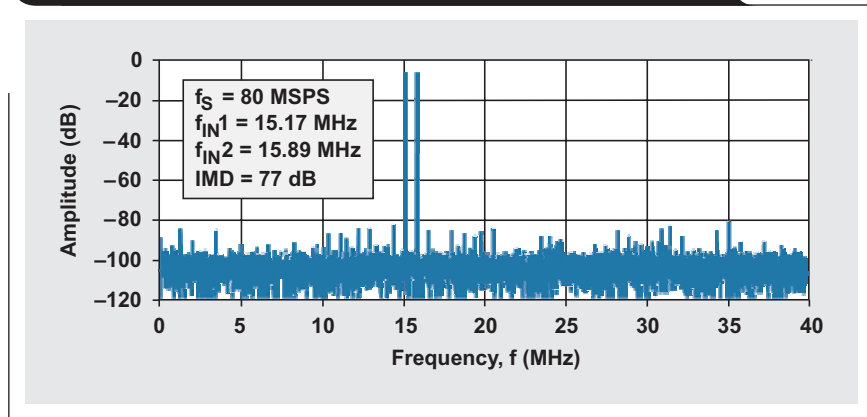
From this it is seen that

$$IIP_3 \text{ (dBm)} = P_{IN} \text{ (dBm)} - \frac{IMD_3 \text{ (dBc)}}{2}. \tag{3}$$

Once we find  $IMD_3$  and know the input power, it is a simple matter to plug them into Equation 3 and calculate  $IIP_3$ .

**Figure 4. Straight-line relationship between  $IMD_3$  and the fundamental**



**Figure 5. Two-tone FFT or spectral plot from Reference 1**

### IP<sub>3</sub> in ADCs

In ADC testing, two tones are applied to the ADC, and the output is examined by taking an FFT or spectral plot to find the two-tone IMD<sub>3</sub>. Figure 5 shows such a plot from Reference 1. The ratio of each of the tones to the IMD<sub>3</sub> product(s) is the two-tone IMD<sub>3</sub> in dBc. IMD<sub>3</sub> depends on signal level. Too high a signal level results in excessive distortion, and too low a signal level makes distortion hard to detect in the presence of noise and other spurious components. An input signal level 7 dB below full-scale input (-7 dBFS) seems to give good results and is commonly used.

Since an ADC is a voltage-driven device, we must choose an input resistance to find the signal power with the formula  $P = V^2/R$ . Assuming that  $FS = 2V_{p-p}$  and  $R = 50 \Omega$ , the full-scale input is +10 dBm. With the input power and the IMD<sub>3</sub>, Equation 3 is used to find IIP<sub>3</sub>.

As an example of how to calculate, consider the following for the ADS5410, a 12-bit ADC. Given that  $FS = 2V_{p-p}$ ,  $R_{IN} = 50 \Omega$ , and  $IMD_3 = 77$  dBc, then

$$IIP_3 = 3 \text{ dBm} - \frac{-77 \text{ dBc}}{2} = 41.5 \text{ dBm}.$$

As mentioned earlier, it is common practice to use a transformer or a fully differential op amp to drive high-performance ADCs differentially. If  $50 \Omega$  is originally used as shown in the example, then the IIP<sub>3</sub> is reduced by  $10 \times \log_{10}(\text{impedance ratio})$ .

For example, if we use a 1:4 impedance ratio (1:2 turns ratio) transformer, the input resistance is  $200 \Omega$  to match to a  $50\text{-}\Omega$  drive amplifier. The IIP<sub>3</sub> is reduced by

$10 \times \log_{10}(200/50) = 6$  dB. Or, if we use a 1:16 impedance ratio transformer with  $800\text{-}\Omega$  input resistance, IIP<sub>3</sub> is 12 dB lower.

### Conclusion

We have examined typical ADC noise and distortion specifications to see how they relate to NF and IP<sub>3</sub>. It is seen that the required information to calculate NF and IP<sub>3</sub> is contained in a typical ADC data sheet.

A key point to remember is that an ADC is a voltage-driven device, whereas NF and IP<sub>3</sub> are associated with power. Thus, in order for the calculations to proceed, an impedance is imposed on the ADC input to find the corresponding power levels.

### References

For more information related to this article, you can download an Acrobat Reader file at [www-s.ti.com/sc/techlit/litnumber](http://www-s.ti.com/sc/techlit/litnumber) and replace "litnumber" with the **TI Lit. #** for the materials listed below.

Document Title	TI Lit. #
1. "12-Bit, 80 MSPS CommsADC™ Analog-to-Digital Converter," Data Sheet, p. 7 . . . . .	slas346
2. Piet Wambacq and Willy Sansen, <i>Distortion Analysis of Analog Integrated Circuits</i> (Kluwer Academic Publishers, 1998).	

### Related Web sites

[analog.ti.com](http://analog.ti.com)  
[www.ti.com/sc/device/ADS5410](http://www.ti.com/sc/device/ADS5410)

# Evaluation criteria for ADSL analog front end

By **John Z. Wu** (Email: wu\_john@ti.com), *Senior Application Engineer, High-Speed Products*, and **C.R. Teeple** (Email: teeple\_cr@ti.com), *Strategic Market Manager, High-Speed Products*

## Introduction

The latest ADSL standard proposed by the International Telecommunication Union (ITU), with the draft recommendation G.992.3-ADSL2, is the next evolution for second-generation ADSL. A summary of the first-generation ADSL evaluation and design criteria is helpful in understanding first-generation ADSL in the mass market and in designing the specifications for second-generation ADSL.

The AFE1302 customer premise equipment (CPE) modem is one practical ADSL analog front end (AFE) design and evaluation example. In this design, an AFE1302 chip and AFE reference design printed circuit board are used for the ADSL CPE modem and CPE PCI card. The maximum reach of the CPE modem is an 18,000-ft (5.5-km) loop with a downstream net bit rate of 928 Kbps and an upstream rate of 416 Kbps.

The maximum transmitted power is defined by ITU G.992 power spectral density (PSD) mask requirements. The crosstalk from coexisting ADSL and ISDN lines can be minimized by limiting the maximum strength of the transmitted ADSL signal power over the twisted-pair long wires. In addition, Electromagnetic Compatibility Society legislation requires that the ADSL transmission system not interfere with AM/FM radio reception. These two requirements place a PSD limit on the strength of the transmitted ADSL signal power.

This article discusses some evaluation and design considerations for addressing transmitted data speed, telephone twisted-pair loop attenuation, the hybrid circuit, and the multitone power ratio (MTPR).

## Transmitted data speed and the total signal-to-noise ratio

Transmitted data speed is the first consideration for ADSL CPE modem design and evaluation. The transmitted data speed is a function of the total signal-to-noise ratio (SNR). The total SNR is the telephone loop SNR plus the modem receive path SNR.

The discrete multitone (DMT) modulation was standardized for the ADSL system by the telecommunication standardization sector of the ITU. For DMT-based ADSL, each subcarrier or tone is spaced at 4.312-kHz intervals. The subcarrier assignment is defined by ITU standard G.992. For example, the subcarrier assignment in G.992.1 annex A can be used for frequency division multiplexing to separate upstream and downstream signals. The subcarriers 31–255 (ITU G.992.1), or subcarriers 31–127 (ITU G.992.2), are reserved for downstream. The subcarriers 0–30—e.g., a maximum total of 31 subcarriers—may be

assigned for upstream. The lowest-frequency subcarriers may be set to zero to allow for voice on the same line, such as in plain old telephone service (POTS).

The lowest-frequency subcarrier used for upstream is determined by the POTS/ADSL splitting filter. The number of upstream and downstream subcarriers is determined by the receive and transmit filters. The actual number of subcarriers employed to modulate data may be less than the maximum and is determined during the initialization sequence. The transmitter designates a subset of the maximum available subcarriers for a connection during the channel analysis phase.

The process of ADSL DMT modulation actually modulates each subcarrier as  $2^{b(i)}$  quadrature amplitude modulation (QAM). The superscript  $b(i)$  denotes the number of bits in the  $i$ th subcarrier. Subcarriers with a lower SNR will be assigned fewer bits to do a small-number QAM constellation. Subcarriers with a higher SNR will be assigned more bits to create a large-number QAM constellation. Suppose that the  $i$ th subcarrier is assigned 8 bits; then the size of the carrier QAM constellation is  $2^8 = 256$  QAM.

The bits are determined by the SNR measured during the channel analysis initialization procedure. The initialization of the CPE modem is performed in five steps: Handshake procedures, channel discovery, transceiver training, channel analysis, and exchange.

During the exchange phase, each receiver communicates to its far-end transmitter the number of bits and relative power levels used on each DMT tone or subcarrier, as well as the final data rate information. After the successful initialization sequence, the transceivers can start communication with actual data.

The channel analysis phase is used to measure the channel characteristics for both directions of transmission. In other words, it measures the channel transfer function versus the frequency response characteristic. The downstream channel characteristics are measured at the CPE side, and the upstream channel characteristics are measured at the central office (CO) side.

During the channel analysis phase, the receiver estimates the transmitted channel gain of each subcarrier in preparation for computing the total SNR for each subcarrier. Then each subcarrier is assigned the number of bits it will carry. The sum of all the bits assigned to all of the subcarriers within the transmitting period (per DMT symbol) determines the transmitted data speed.

The number of bits assigned per subcarrier can be calculated by

$$b(i) = \log_2[1 + \text{snr}(i) \times g/\gamma \times m]. \quad (1)$$

Further,  $2^{b(i)} - 1 = \text{snr}(i) \times g/\gamma \times m$ , and

$$10\log_{10}[2^{b(i)} - 1] \\ = 10\log_{10}[\text{snr}(i)] + 10\log_{10}(g) - 10\log_{10}(\gamma) - 10\log_{10}(m).$$

Only if  $2^{b(i)} \gg 1$  is the following equation true:

$$10\log_{10}[2^{b(i)}] = \text{SNR (dB)} + G \text{ (dB)} - \Gamma \text{ (dB)} - M \text{ (dB)}.$$

Therefore,

$$b(i) = [\text{SNR (dB)} + G \text{ (dB)} - \Gamma \text{ (dB)} - M \text{ (dB)}]/3 \text{ dB (bits)}. \quad (2)$$

Variable definitions for the preceding equations are as follows:

- $b(i)$  is the number of bits in the  $i$ th subcarrier.
- $i$  is the subcarrier index from 0 to  $N - 1$ ;  $N$  is the total usable subcarrier number; and the maximum  $N = 256$ .
- $\text{snr}(i)$  is the SNR per subcarrier; it is a real value that represents the ratio between the received signal power and the received noise power for that subcarrier.  
 $\text{SNR (dB)} = 10\log_{10}[\text{snr}(i)]$ .
- $\gamma$  or  $\Gamma$  is a constant determined by the required bit error rate (BER). For example,  $\gamma = 9.55$  and  $\Gamma = 10\log_{10}(\gamma) = 9.8$  (dB) for  $\text{BER} \leq 10^{-7}$ .
- $g$  or  $G = 10\log_{10}(g)$  (dB) is a gain provided by Reed-Solomon error correction coding to make the system robust against impulsive noise bursts.  
 $\text{SNR (dB)} = 10\log_{10}[\text{snr}(i)]$ .
- $m$  or  $M = 10\log_{10}(m)$  (dB) is the margin to represent the amount of increased noise relative to the noise power that the system is designed to tolerate and still meet the target BER of  $10 \times e^{-7}$ , accounting for all coding (trellis coding and Reed-Solomon forward error correction) gains included in the design. This margin can prevent too many bits from swapping if the SNR changes. Normally  $M = 6$  dB is used to prevent online swapping.

$G$  (dB),  $\Gamma$  (dB), and  $M$  (dB) are constants. One bit is added to the assigned  $b(i)$  if SNR (dB) increases 3 dB in the subcarrier channel; this is the “one-bit-per-3-dB” rule.

Assuming that  $G$  (dB) = 2 dB,  $\Gamma$  (dB) = 9.8 dB, and  $M$  (dB) = 6 dB, a typical  $b(i)$  and SNR (dB) versus the tone number is shown in Figure 1.

The transmitted data speed can be calculated by

$$C = [\sum b(i)]/t \text{ for } i = 0 \text{ to } N - 1,$$

where  $C$  is the transmitted data speed and  $t$  is the transmission period.

*Example 1:* If the gain of trellis and Reed-Solomon coding is not included, the attainable net rate or the maximum data rate is

$$C = \{\sum [\text{SNR (dB)} - \Gamma \text{ (dB)} - M \text{ (dB)}]/3 \text{ dB}\}/t \text{ (bps)}$$

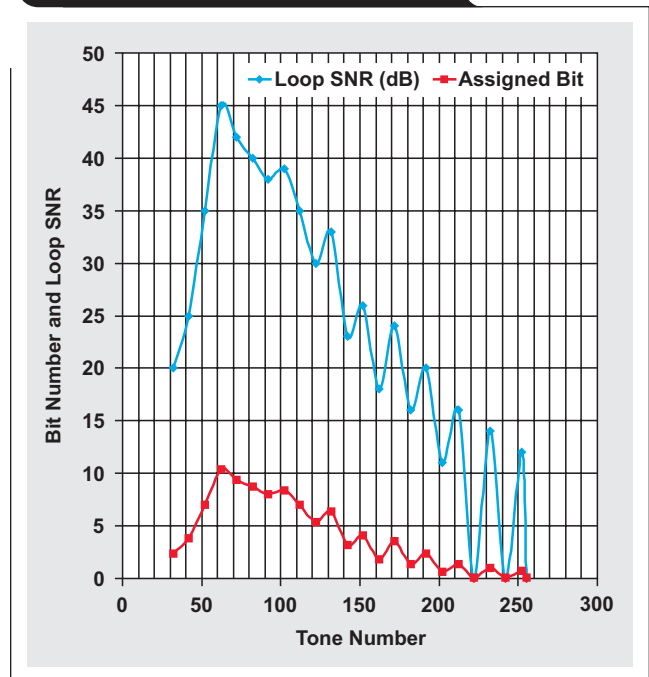
for  $i = 0$  to  $\text{NSC} - 1$ , where  $\text{NSC}$  is the number of subcarriers.

*Example 2:* Additionally, if  $M = 6$  dB and  $G = 6$  dB, the attainable net rate can be simplified as follows:

$$C = \{\sum [\text{SNR}(i) - \Gamma]/3 \text{ dB}\}/t \text{ (bps)}$$

for  $i = 0$  to  $\text{NSC} - 1$ . For the duration of a DMT symbol,  $t = 250 \mu\text{s}$ . The data symbol rate (4000 data symbols/second) is the net average rate at which symbols carrying data frames are transmitted. However, in order to insert

**Figure 1. Bit assignment and loop SNR relationship**



the synchronization symbol, the symbol rate is defined as the rate at which all symbols, including the synchronization symbol, are transmitted; that is,  $(69/68) \times 4000 = 4058.8$  symbols/second.

From the equation given earlier, the transmitted data speed is determined by the total SNR. The modem RX path noise is not covered in this article. The transmitted DMT signal power and loop noise are specified in the recommended ITU G.992 as follows:

- For G.992.1, the downstream PSD is  $-40$  dBm/Hz, from 25.875 to 1104 kHz, for a total transmission power not greater than 20.4 dBm if all subcarriers are used.
- For G.992.2, the downstream PSD is  $-40$  dBm/Hz, from 25.875 to 552 kHz, for a total transmission power not greater than 16.2 dBm if all subcarriers are used.
- The upstream normal transmit PSD, for the channel analysis signal (R-REVERB1) and all subsequent upstream signals, is  $-38$  dBm/Hz, which is equivalent to  $-1.65$ -dBm total transmit power in any 4.3125-kHz subcarrier. The maximum transmit PSD should be no higher than  $-37$  dBm/Hz, for an aggregate transmit power not greater than 12.5 dBm if all subcarriers are used.
- The telephone loop noise is assumed to be  $31.62 \text{ nV}/\sqrt{\text{Hz}}$ , or  $-140$  dBm/Hz. It is specified as the quiet line noise PSD  $N(f)$  for a particular subcarrier in G.992.3-ADSL2; and it is the rms level of the noise present on the telephone line when no ADSL signals are present on the line.

A practical evaluation result of the transmission channel capacity is the net data speed for the AFE1302 CPE

modem. The evaluation is based on using the subcarriers 36–127 for downstream with a total transmission power of less than 15.99 dBm during the training phase and less than 6.06 dBm during the SHOWTIME state. The SHOWTIME state is the normal operation state after all initialization and training are completed. Taking into account all noise contributions, the loop noise test results referred to the telephone line are less than  $-148$  dBm/Hz over receiver bandwidth for the AFE1302 CPE modem. The tested downstream net bit rate can reach 928 Kbps with an 18,000-ft (5.5-km) loop. For the test environments, the loop simulator NSA400 is set as a 26-AWG twisted-pair telephone wire without a bridged tap, the noise margin is 6 dB, and the interleave depth is 16 with no trellis coding.

### Twisted-pair telephone-loop attenuation

The reach of an ADSL system is the distance over telephone lines that it can transmit and receive information. Reach is the key performance parameter for ADSL and is limited by twisted-pair telephone-loop attenuation.

Telephone-loop attenuation is defined as the difference between the total maximum transmitted power at one end of the telephone line and the total received power at the other end of the line. Loop attenuation is mainly dictated by wire diameters, loop length, and the transmitted signal frequency. The most frequently used telephone twisted-wire diameters are 0.4 mm for 26-AWG wire and 0.5 mm for 24-AWG wire. The typical loop length varies from 6,000 to 18,000 ft (1.8 to 5.5 km) in North America, Europe, and Asia. ADSL signals cover the bandwidth of 25.875 kHz to 1104 kHz as specified in ITU G.992.

According to POTS application statistics, the typical voice signal loss through a telephone loop is 3 to 6 dB per mile (1.6 km) within the voice bandwidth of 300 Hz to 4 kHz. Because ADSL signal frequency is much higher than the POTS signal, and because line attenuation increases as signal frequency increases, the loop attenuation is greater within the ADSL signal bandwidth.

The transfer function of a twisted-pair telephone loop is dominated by the skin effect: High-frequency currents tend to flow only in the outer portion, or skin, of the conductor, resulting in an increase of the attenuation at higher frequencies. In the case of a twisted-pair loop, the attenuation is a function approximately proportional to  $f^{1/4}$  for frequencies below 350 kHz, and approximately proportional to  $f^{1/2}$  for frequencies above 350 kHz.

The experimental data in Figure 2 shows that the loop attenuation increases from around 5 dB per 3300 ft (1 km) at 10 kHz to over 15 dB per 3300 ft (1 km) at 1 MHz. This means that a 13,100-ft (4-km), 24-AWG twisted-pair telephone loop has an attenuation of over 20 dB at 100 kHz, and over 70 dB at 1 MHz. Over the ADSL signal bandwidth, the twisted-pair loop attenuation varies by more than 50 dB.

During channel analysis, the CO-side receiver calculates the average loop attenuation. Based on the channel analysis signal (R-REVERB1) using subcarriers 7–18, the average upstream loop attenuation is calculated as the difference between the total transmitted power at the CPE side and the total received power measured at the CO side. In G.992.3-ADSL2, for a given loop length, the loop attenuation is defined as

$$\text{LATN (dB)} = 10 \times \log[\Sigma |H(f)|^2 / \text{NSC}]$$

for  $i = 0$  to  $\text{NSC} - 1$ . Variables for this equation are defined as follows:

- NSC is the number of subcarriers.
- $H(f)$  is the channel characteristic function per subcarrier.
- LATN is the difference in decibels between the power received at the near end and that transmitted from the far end over all subcarriers; its dynamic range is from 0 to 102.2 dB.

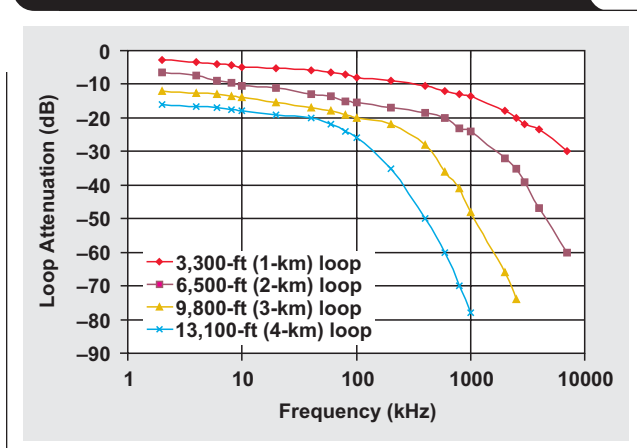
For example, assume that  $\text{LATN} = 58.2$  dB,  $N = -140$  dBm/Hz,  $G = M = 6$  dB, the transmitted signal power is  $-30$  dBm/Hz, and the received signal power is  $S = -88.2$  dBm/Hz for a particular subcarrier. With Equation 2,  $b(i)$  can be calculated as 14 bits, which means that 14 bits of data can be assigned on that subcarrier. But if LATN increases to 88.2 dB for a longer loop, then  $b(i)$  is only 4 bits because of the one-bit-per-3-dB rule.

A longer-reach loop and a higher subcarrier frequency result in greater loop attenuation, which means that fewer data bits can be assigned to subcarriers, and lower data speed can be achieved.

### Hybrid circuit

The ADSL hybrid circuit is a three-port network used to pass the transmit signal from the AFE transmission port to the telephone-loop port and to pass the receive signal from the telephone loop port to the AFE receive port. The ADSL hybrid circuit is also used to eliminate the transmit signal from the receive signal in the receive path. It allows full-duplex transceiver operation in a twisted-pair telephone loop. ADSL hybrid echo return loss is the amount of attenuation between the transmitted signal power and the reflected echo power in the receive path, normally

**Figure 2. A 24-AWG twisted-pair telephone-loop attenuation vs. frequency**



expressed in decibels. It is a key target of evaluation and design for an ADSL AFE. The higher the echo return loss, the less of the transmitted signal power gets into the receive path.

$$H_{\text{echo}} = 10 \times \log(P_{\text{echo}}/P_{\text{tx}}),$$

where  $H_{\text{echo}}$  is the hybrid echo return loss,  $P_{\text{tx}}$  is the transmitted signal power, and  $P_{\text{echo}}$  is the portion of transmitted power that enters the receive channel (also called the reflected echo power in the receive path).

The actual twisted-pair loop impedance  $Z(f)$  is the frequency function of the telephone line. The magnitude of the twisted-pair impedance is about 600  $\Omega$  for the POTS bandwidth; but for the ADSL signal bandwidth, it is about 100  $\Omega$  without bridged taps and varies from 60 to 100  $\Omega$  with bridged taps.

The hybrid circuit used in the AFE1302 CPE modem is purely resistive and basically an electrical bridge circuit. When the differential drive resistive network becomes balanced, the amount of hybrid echo is minimized.

In a DMT-based ADSL system, the ADSL hybrid circuit and the receive path filter are the critical factors for receiver performance. The transmit path signal and noise power need to be sharply attenuated by the hybrid echo path and receive filter. They can significantly improve CPE modem reach and downstream data speed.

For the typical value of 100- $\Omega$  equivalent twisted-pair loop impedance, a total 40-dB attenuation of a hybrid circuit and receive high-pass filter is the minimum evaluation and design requirement. A 20-dB return loss can be easily achieved through the hybrid circuit. The hybrid plus the third-order, LC RX filter on-board can provide a total echo loss of more than 40 dB. That is, the hybrid circuit can attenuate the transmitted power and noise by 40 dB (see Figure 3).

## The multitone power ratio

The multitone power ratio (MTPR) is an important feature in the evaluation and design of DMT-based ADSL systems. Better MTPR performance in both the transmission and receive paths results higher data rates in the ADSL system.

The MTPR is the ratio of the power in one subcarrier to the noise power in another selected empty subcarrier. There are no data bits assigned to the selected empty subcarrier in a DMT modulation. The MTPR indicates the degree to which a subcarrier QAM signal is corrupted by distortion from all other subcarrier QAM signals.

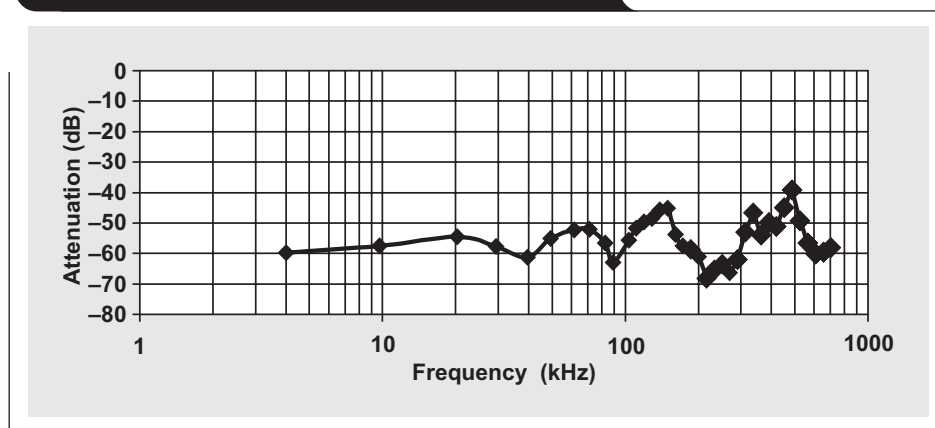
The measurement and evaluation for this kind of corruption are different from that for traditional single-tone distortion. Signal-to-noise and distortion ratio (SINAD), spurious-free dynamic range (SFDR), single-tone harmonic distortion, two-tone intermodulation distortion (IMD), third-order intercept point ( $IP_3$ ), and total harmonic distortion (THD) are used only for expressing single- or two-tone signal integrity and spectral properties.

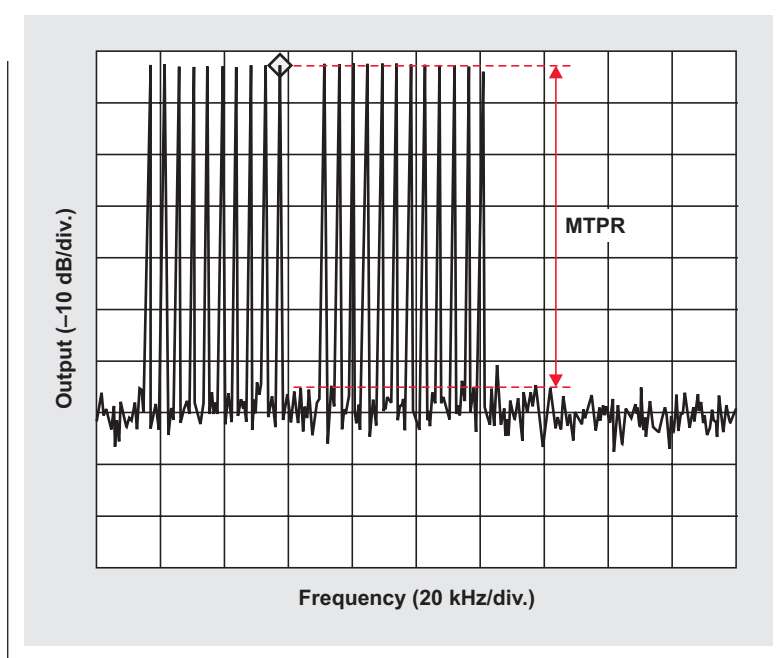
The MTPR, on the other hand, indicates how the tested device—such as line driver, receiver, line transformer, TX filter, RX filter, or DAC/ADC—responds to the discrete multitone signal, which is not 1 or 2 tones but may be up to 255 or more.

One of the design tasks for the ADSL CPE modem is to maintain the fidelity of the discrete multitone signal. All the analog components used on the modem—such as line transformer, common-mode choke, hybrid circuit, TX filter, RX filter, and line driver and receiver—must be designed so that they cause minimal corruption of the discrete multitone signal.

For any subcarrier, the minimum transmitter MTPR shall be at least 38 dB as specified in G.992, and at least 44 dB as recommended by G.992.3.

**Figure 3. Hybrid echo return loss plus RX filter attenuation vs. frequency**



**Figure 4. Transmitter path MTPR performance of AFE1302**

The MTPR of a tested device can be measured as the dynamic range from peak power in a subcarrier to the peak distortion in an empty tone. For example, a test result shows that an MTPR of 65.82 dB can be achieved in the AFE1302 CPE modem transmission path. The test tool is National Instruments PXI-1002 arbitrary waveform generator 5411.

The transmitter path is defined as the path from the DSP interface TX output to the twisted-pair telephone line interface with 100- $\Omega$  impedance (see Figure 4). The transmitted multitone signal is from tones 6–29 and with notch tones 16 and 17. The internal AFE1302's TX programmable gain amplifier gain is 0 dB, and the external TX line driver gain is 15 dB. The tested result of the MTPR is 65.82 dB.

### Summary

This article has discussed some evaluation and design considerations for an ADSL AFE. The most critical evaluation criterion is an ADSL transceiver data speed that is limited by the total SNR. The second issue is frequency variation of telephone-loop attenuation and its impact on reach. This article further pointed out that the improvement on

hybrid echo return loss significantly increases the received data speed and the reach. The MTPR, a kind of corruption that differs from the traditional single-tone distortion, is another important criterion for designing and evaluating an ADSL AFE.

### References

For more information related to this article, you can download an Acrobat Reader file at [www-s.ti.com/sc/techlit/litnumber](http://www-s.ti.com/sc/techlit/litnumber) and replace "litnumber" with the **TI Lit. #** for the materials listed below.

- | <b>Document Title</b>   | <b>TI Lit. #</b> |
|---|------------------|
| 1. "ITU-T Draft Recommendation G.992.3-ADSL2," International Telecommunication Union, Geneva, Switzerland, April 29–May 10, 2002. | —                |
| 2. "ADSL Analog Front-End," Data Sheet . . . . .sbws014   | —                |

### Related Web sites

[analog.ti.com](http://analog.ti.com)  
[www.ti.com/sc/device/AFE1302](http://www.ti.com/sc/device/AFE1302)

# UCC28517 100-W PFC power converter with 12-V, 8-W bias supply, Part 2

By Michael O'Loughlin (Email: michael\_oloughlin@ti.com)

Member, Applications Engineering Staff

## Introduction

Power factor corrected (PFC) preregulators are generally used in offline ac/dc power converters with a power level higher than 75 W or to meet line harmonic requirements such as EN61000-3-2. PFC is typically done with a boost converter ac/dc topology due to the continuous input current that can be manipulated through average current-mode control to achieve a near-unity power factor (PF). However, due to the high output voltage of a boost converter, a second dc/dc converter is generally needed to step down the output to a usable voltage. In the past this has been accomplished with two pulse-width modulators (PWMs). One PWM controlled and regulated the PFC

power stage, while the second was used to control the step-down converter. The UCC28517 controller reduces the need for two PWMs and combines both of these functions into one control-integrated circuit. The UCC28517 operates the second converter at twice the switching frequency of the PFC stage, which reduces the size of the boost magnetics and the ripple current in the boost capacitor. For more information on this device, please see Reference 7. This article reviews the design of the second 12-V, 8-W power stage to be used as an auxiliary bias supply. A review of the PFC preregulator power stage can be found in the 3Q03 issue of the *TI Analog Applications Journal*.

## Variable definitions

$\Delta t$	Soft-start interval	$P_{DIODE\_CAP}$	Loss due to boost diode capacitance
$\eta_1$	Output A efficiency	$P_{FET\_TR}$	FET transition losses
$\eta_2$	Output B efficiency	$P_{GATE}$	Power dissipated by the FET gate
$C_{DIODE}$	Boost diode capacitance	$P_{OUTA}$	Output A maximum power
$C_{OSS}$	FET drain-to-source capacitance	$P_{OUTB}$	Output B maximum power
$D_{max}$	Duty cycle maximum	$Q_{GATE}$	FET gate charge
$ESR$	Output capacitance equivalent resistance	$R_{DS(on)}$	On resistance of the FET
$f_c$	Voltage-loop crossover frequency	$R_{load}$	Typical load impedance
$f_{opto\_pole}$	Frequency where optoisolator gain is -3 dB from its dc operating point	$R_{SENSE}$	Current sense resistor
$f_s$	Minimum switching frequency	$s$	Angular frequency ( $j2\pi f$ )
$f_{SA}$	Output A switching frequency	$t_{blank}$	Amount of leading-edge blanking time
$f_{SB}$	Output B switching frequency	$t_f$	FET fall time
$G_{c(s)}$	Control transfer function	$t_r$	FET rise time
$G_{co(s)}$	Control to output transfer function	$T_{SB}$	$1/f_{SB} = 5 \mu s$
$G_{opto(s)}$	Optoisolator gain transfer function	$T_{s(f)}$	Voltage loop frequency response
$H_{(s)}$	Voltage divider gain	$V_{boost}$	Same as $V_{OUTA}$
$I_m$	Transformer magnetizing current	$V_c$	Control voltage
$I_{op\_min}$	Minimum optocoupler current (1 mA)	$V_{ct}$	Oscillator peak (5 V)
$I_{PK}$	Peak inductor current, peak diode current, peak switch current	$V_d$	Forward diode drop (0.6 V)
$I_{RMS}$	RMS device current	$V_{dynamic}$	Current sense voltage range
$I_{SS}$	UCC28517 soft-start current of 10 $\mu A$	$V_f$	Forward voltage of a diode
$L_m$	Transformer primary magnetizing inductance	$V_{GATE}$	Gate-drive voltage
$N$	Transformer turns ratio	$V_{IN}$	RMS input voltage
$N_p$	Primary turns	$V_{OUTA}$	Boost output voltage ( $V_{boost}$ )
$N_s$	Secondary turns	$V_{OUTB}$	Auxiliary output voltage
$P_{COND}$	Device conduction losses	$V_{pp}$	Output peak-to-peak ripple voltage
$P_{COSS}$	Power dissipated by the FET's drain-to-source capacitance	$V_{REF}$	UCC28517 internal reference
$P_{DIODE}$	Total loss in the boost diode	$V_{ripple}$	Output B ripple voltage
		$V_{slope}$	Voltage ramp peak added for slope compensation
		$V_{VERR}$	Feedback error voltage
		$V_{VREF\_TL431}$	TL431 (D13) internal reference



Figure 2. dc/dc power stage schematic

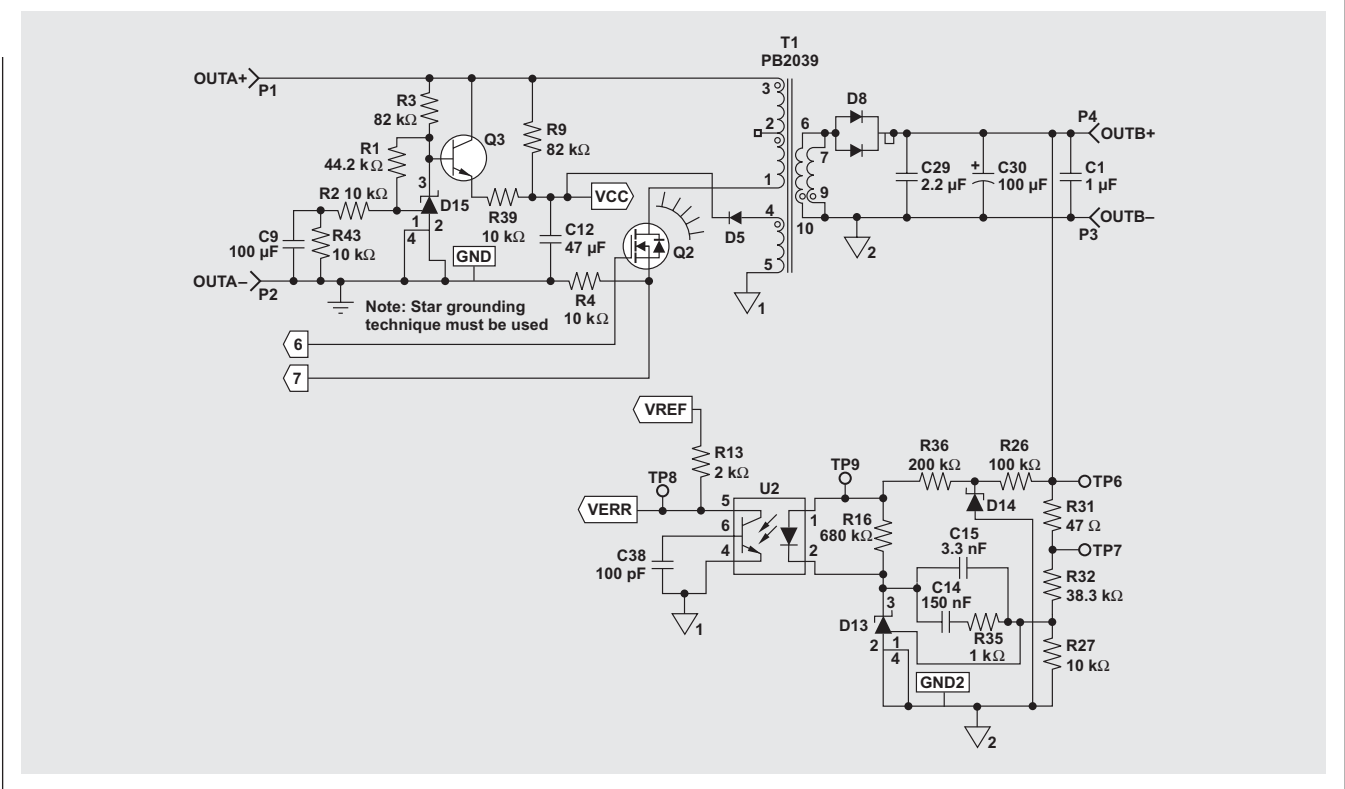
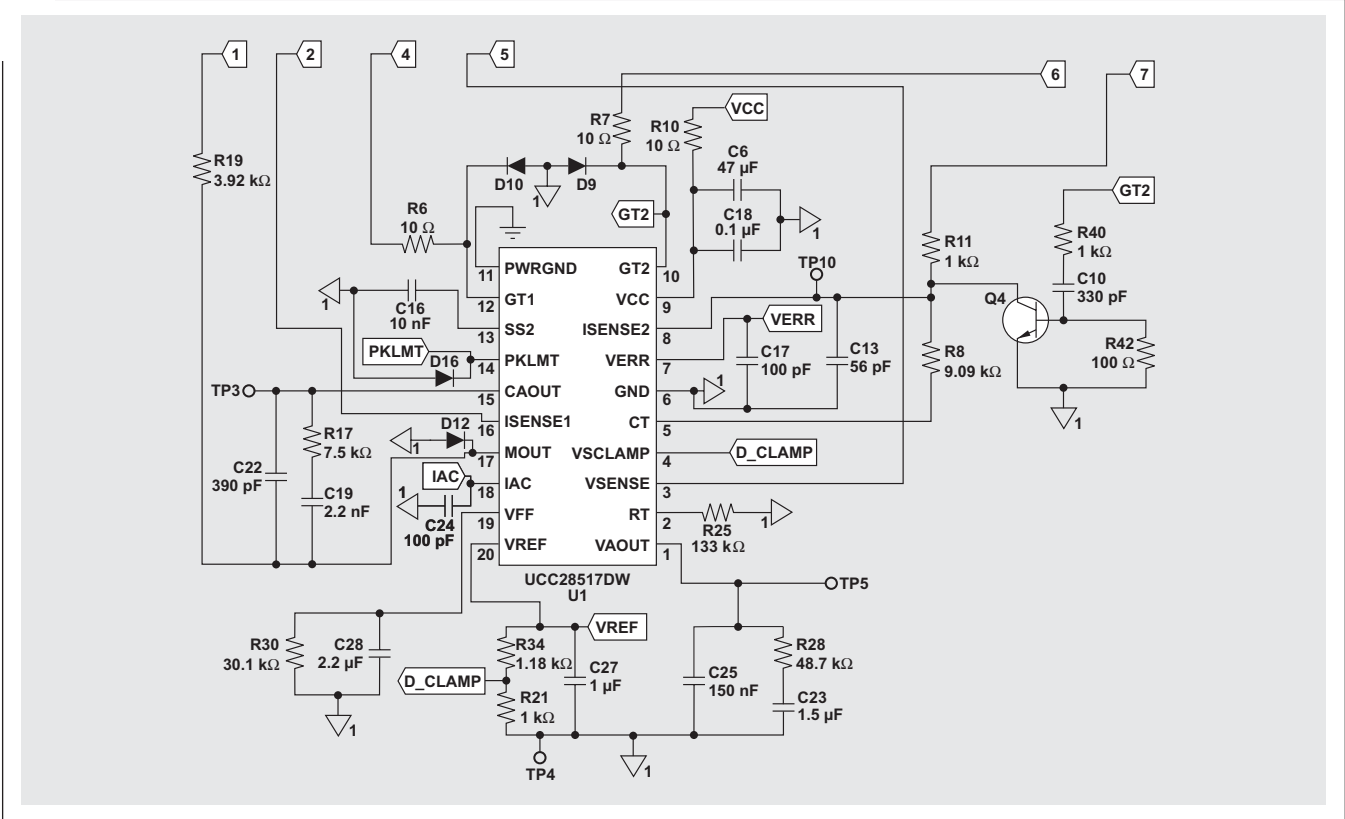


Figure 3. Controller schematic



operate during loss of line voltage. An auxiliary winding of 22 turns was added to power the UCC28517 control IC as well. For this design Pulse Engineering designed a 22-turn transformer (part number PB2039).

### Power switch (Q2) and output diode (D8) selection

To select D8 and Q2 properly, a power budget is generally set for these devices to maintain the desired efficiency goal. The following equations were used to estimate power loss in the switching devices. To meet the power budget for this design, an IRFBBF20S FET and a 20CJQ045 dual diode from International Rectifier were chosen.

$$I_{PK\_Q2} = \frac{2 \times \frac{P_{OUTB}}{V_{OUTB}}}{\eta 2 \times N}$$

$$I_{RMS\_FET\_Q2} = \frac{P_{OUTB}}{\eta 2 \times N} \times \sqrt{\frac{D_{max}}{3}}$$

$$P_{COND\_FET\_Q2} = R_{DS(on)} \times I_{RMS\_FET}^2$$

$$P_{GATE\_Q2} = Q_{GATE} \times V_{GATE} \times f_S$$

$$P_{COSS\_Q2} = \frac{1}{2} C_{OSS\_Q2} \times V_{OUTB}^2 \times f_S$$

$$P_{FET\_TR\_Q2} = \frac{1}{2} V_{OUTB} \times I_{RMS\_Q2} \times (t_r + t_f) \times f_{SB}$$

$$P_{Q2} = P_{GATE\_Q2} + P_{COSS\_Q2} + P_{COND\_FET} + P_{FET\_TR\_Q2}$$

$$I_{PK\_D8} = \frac{2 \times P_{OUTB} \times (1 - D_{max})}{V_{OUTB}}$$

$$P_{DIODE\_CAP\_D8} = \frac{C_{DIODE}}{2} \times V_{OUTB}^2 \times f_{SB}$$

$$P_{COND\_D8} = V_f \times I_{RMS\_D8}$$

$$I_{RMS\_D8} = I_{PK\_D8} \times \sqrt{\frac{1 - D_{max}}{3}}$$

$$P_{DIODE} = P_{COND\_D8} + P_{DIODE\_CAP\_D8}$$

### Output capacitor

The output capacitor selection for the step-down converter was based on requirements for energy storage, output ripple voltage, RMS current, and peak current.

$$I_{PK\_C30} = 2 \times \frac{\frac{P_{OUTB}}{V_{OUTB}}}{1 - D_{max}}$$

$$ESR_{C30\_max} \leq \frac{V_{ripple}}{I_{PK\_C30}}$$

$$C30 \geq \frac{0.5 \times I_{PK} \times (1 - D_{max})}{f_{SB} \times V_{OUTB}}$$

$$I_{RMS\_C30} = I_{PK\_C30} \times \sqrt{(1 - D_{max}) \times \left[ \frac{4 - 3 \times (1 - D_{max})}{12} \right]}$$

### R<sub>SENSE2</sub>

The dc/dc power converter is designed for peak-current-mode control. R4 is the current sense resistor, which can be sized through the following two equations.

$$I_m = \frac{V_{OUTA} \times D_{max}}{L_m \times f_{SB}}$$

$$R4 = \frac{V_{dynamic}}{I_m + \frac{I_{PK\_C30}}{N}}$$

### Soft start

The UCC28517 has soft-start circuitry to allow for a controlled ramp of the second stage's duty cycle during startup. The following equation was used to calculate the approximate capacitance needed to achieve a soft start of roughly 5 ms ( $\Delta t$ ).

$$C16 = \frac{I_{SS} \times \Delta t}{5 \text{ V}}$$

### Slope compensation

Designing a power converter that uses peak-current-mode control generally requires slope compensation to remove instabilities in the control loop and to make the design less susceptible to noise. Resistors R11 and R8 (Figure 3) sum in a portion of the oscillator signal to the current sense signal for slope compensation. Generally the added slope ( $V_{slope}$ ) required is equal to half the down slope of the change in output current. By selecting R11 first, you can calculate the required value of R8 to generate the required slope compensation.

$$V_{slope} = \left( I_m + \frac{I_{PK\_C30}}{2N} \right) R4$$

$$R8 \leq \frac{R11(V_{ct} - V_{slope})}{V_{slope}}$$

### Leading-edge blanking circuit

The typical current sense signal for a converter using peak-current-mode control is shown in Figure 4. As shown, during time T1 there is a leading current spike. This is partly caused by the parasitic gate-to-source capacitance of the power stage switch Q4 and the voltage divider formed off the gate drive by R4 and R7. This leading-edge spike can cause the peak-current-mode signal to terminate the gate drive prematurely. To remove this instability, a leading-edge blanking circuit was constructed.

Electronic components Q4, R40, R42, and C10 form a leading-edge blanking circuit. This circuit is used to clamp leading-edge current spikes. The timing of the leading-edge blanking can be adjusted by modifying the size of timing capacitor C10:

$$C10 = \frac{t_{blank}}{2(R40 + R42)}$$

### Control loop for the dc/dc converter

Figure 5 shows the control block diagram for the control loop of the dc/dc converter.  $G_c(s)$  is the compensation network's transfer function (TF),  $G_{opto(s)}$  is the optoisolator gain TF,  $G_{co(s)}$  is the control-to-output gain TF, and  $H(s)$  is the divider gain TF. To estimate the frequency response of each gain block, the following equations can be used.  $f_{opto\_pole}$  is the frequency where the optoisolator gain is -3 dB from its dc operating point; and  $V_{VREF\_TL431}$  is the internal reference voltage of the TL431 shunt regulator.  $R_{load}$  represents the typical load impedance for the design.

$$H(s) = \frac{R27}{R27 + R32} = \frac{V_{VREF\_TL431}}{V_{OUTB}}$$

$$G_{opto(s)} = \frac{R13}{R36} \times \frac{1}{1 + \frac{s}{2\pi f_{opto\_pole}}}$$

$$G_c(s) = \frac{s \times R35 \times C14 + 1}{s \times C14 \times R31 \times (1 + s \times R35 \times C15)} \times \frac{R13}{R36} \times \frac{1}{1 + \frac{s}{2\pi f_{opto\_pole}}}$$

$$G_{co(s)} = \frac{V_{OUTB}}{V_c} = \frac{R_{load}}{R4} \times \frac{N_p}{N_s} \times \frac{1 + s \times C30 \times ESR}{1 + s \times C30 \times R_{load}}$$

Figure 4. Typical current sense signal

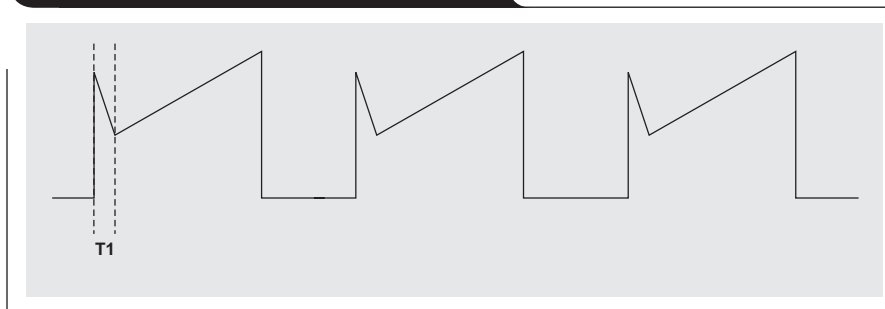


Figure 5. dc/dc converter control loop

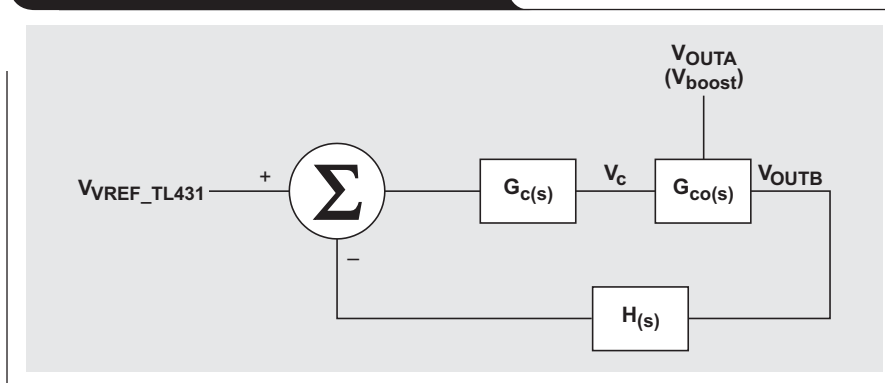
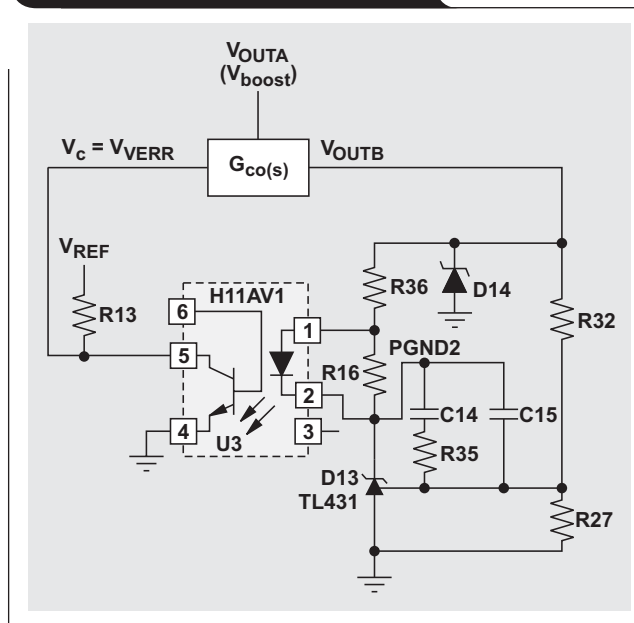


Figure 6 shows the circuitry that was used for the voltage feedback loop. D13 is a TL431 shunt regulator that can function as an operational amplifier to provide feedback control when set up in this configuration.

Figure 6. Voltage feedback loop



Initially the resistor values for the divider gain,  $H_{(s)}$ , must be selected. The following equation can be used to size these resistors, where  $V_{OUTB}$  is the desired output voltage and  $V_{VREF\_TL431}$  is the internal reference of the TL431.

$$R32 = \frac{R27(V_{OUTB} - V_{VREF\_TL431})}{V_{VREF\_TL431}}$$

It is important to bias the TL431 and the optoisolator correctly for proper operation. Resistors R16 and R13 provide the minimum bias currents for the TL431 and the optoisolator, respectively, and can be selected with the following equations. The optoisolator was configured to have a dc gain of roughly 20 dB, and the optoisolator had a crossover frequency of roughly 80 kHz. Figure 7 shows the small signal frequency response of the optoisolator.

$$R16 = \frac{V_f}{I_{TL431\_min}}$$

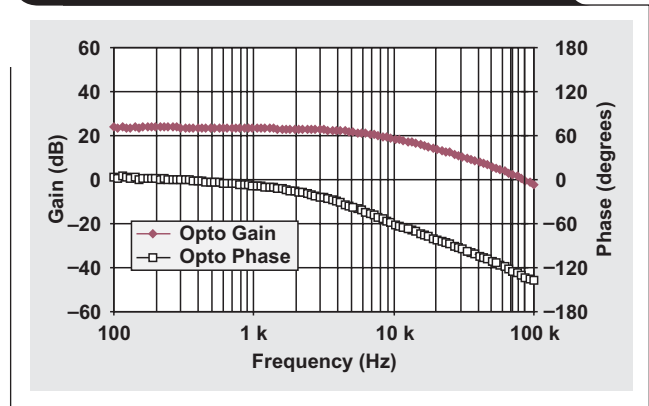
$$R13 = \frac{V_{REF} - V_{VERR(max)}}{I_{op\_min}}$$

Before attempting to compensate the control loop,  $T_{s(f)}$ , we must define some design goals for the closed-loop frequency response. Typically the loop is designed to cross over at a frequency below one-sixth of the switching frequency (see Reference 3). For this design example to have good transient response, the design goal was to have the loop gain crossover frequency ( $f_c$ ) at roughly 1 kHz, which is less than one-sixth of the switching frequency ( $f_{SB}$ ). The following equation describes the frequency response of the system loop gain,  $T_{s(f)}$ , in decibels.

$$T_{s(f)} = G_{c(s)dB} + G_{co(s)dB} + H_{(s)dB}$$

The compensation network that is used ( $G_{c(s)}$ ) has three poles and one zero. One pole occurs at the origin, and a second pole is caused by the limitations of the optoisolator. The third pole is set at one-half the switching frequency to attenuate the high frequency gain. The zero

Figure 7. Optoisolator frequency response



is set at the desired crossover frequency. The following equations can be used to select R35, C14, and C15 of  $G_{c(s)}$  to obtain the desired design goals.

$$H_{(s)dB} = 20 \log(H_{(s)})$$

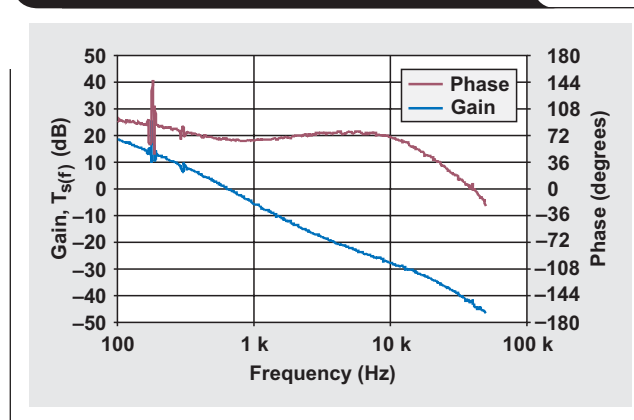
$$R35 = R32 \times 10^{\frac{-(G_{co(s)dB} + G_{opto(s)dB} + H_{(s)dB})}{20}}$$

$$C14 = \frac{1}{2 \times \pi \times R35 \times f_c}$$

$$C15 = \frac{1}{2 \times \pi \times R35 \times \frac{f_s}{2}}$$

Figure 8 shows the measured loop gain frequency response,  $T_{s(f)}$ . The frequency response characteristics in Figure 8 show that  $f_c$  was roughly equal to 800 Hz with a phase margin of roughly 50°. It is important to note that the equations used to compensate the control loop by selecting C14, C15, and R35 are estimates and the values may have to be adjusted to get the appropriate compensation.

Figure 8. Frequency loop response,  $T_{s(f)}$



### Summary

In this design example we reviewed the design of a 100-W PFC ac/dc preregulator with an auxiliary 12-V, 8-W bias supply. The UCC2851x family of combination PWM controllers is perfect for offline applications that require PFC and auxiliary power supplies to meet different system requirements. The design performance of this two-stage power converter is shown in Figures 9–12.

### References

For more information related to this article, you can download an Acrobat Reader file at [www-s.ti.com/sc/techlit/litnumber](http://www-s.ti.com/sc/techlit/litnumber) and replace “litnumber” with the **TI Lit. #** for the materials listed below.

Document Title	TI Lit. #
1. Laszlo Balogh, “Design Review: 140W, Multiple Output High Density DC/DC Converter,” p. 6-9	.slup117
2. Laszlo Balogh, “Unitrode – UC3854A/B and UC3855A/B Provide Power Limiting With Sinusoidal Input Current for PFC Front Ends,” Unitrode Design Note	.slua196
3. Lloyd Dixon, “Control Loop Cookbook,” p. 5-17	.slup113
4. Lloyd Dixon, “Optimizing the Design of a High Power Factor Switching Preregulator,” pp. 7-11–7-12	.slup093
5. James P. Noon, “A 250kHz, 500W Power Factor Correction Circuit Employing Zero Voltage Transitions,” pp. 1-11–1-14	.slup106
6. “Practical Considerations in Current Mode Power Supplies,” Unitrode Application Note	.slua110
7. “Advanced PFC/PWM Combination Controllers,” Data Sheet	.slus517
8. “UCC28517 EVM User’s Guide”	.sluu117

### Related Web sites

[analog.ti.com](http://analog.ti.com)  
[www.ti.com/sc/device/TL431](http://www.ti.com/sc/device/TL431)  
[www.ti.com/sc/device/UCC28517](http://www.ti.com/sc/device/UCC28517)

Figure 9. Output A THD vs. output power

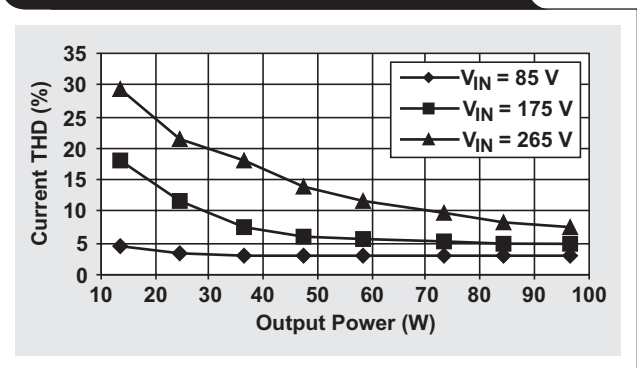


Figure 10. Output A efficiency vs. output power

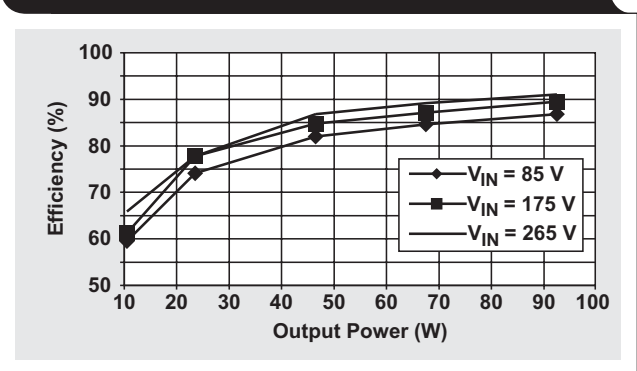


Figure 11. Output A PF vs. output power

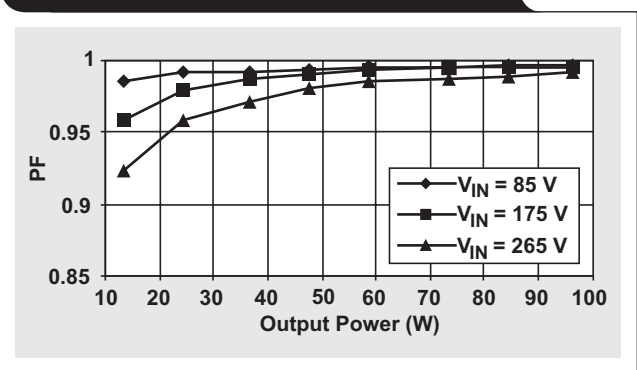
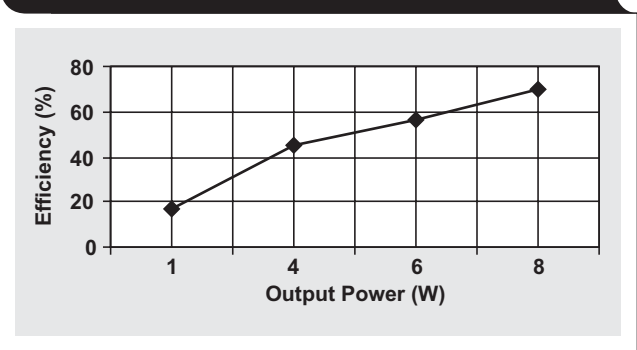


Figure 12. Output B efficiency vs. output power



# Calculating noise figure in op amps

By James Karki (Email: j-karki@ti.com)

Member, Group Technical Staff, High-Performance Linear

## Introduction

Noise figure is commonly used in communications systems because it provides a simple method to determine the impact of system noise on sensitivity.

Today, the performance of wide-band op amps is making them viable alternatives to more traditional open-loop amplifiers like monolithic microwave integrated circuits (MMICs) and discrete transistors in communications design.

Recognizing the need to specify wide-band op amps in RF engineering terminology, some manufacturers do provide noise figure, but they seem to be the exception rather than the rule.

Op amp manufacturers typically specify noise performance by giving the input-referred voltage and current noise. The noise figure depends on these parameters, the circuit topology, and the value of external components. If you have all this information, noise figure can be calculated.

## Review of noise figure

Noise figure (NF) is the decibel equivalent of noise factor (F):  $NF \text{ (dB)} = 10\log(F)$ .

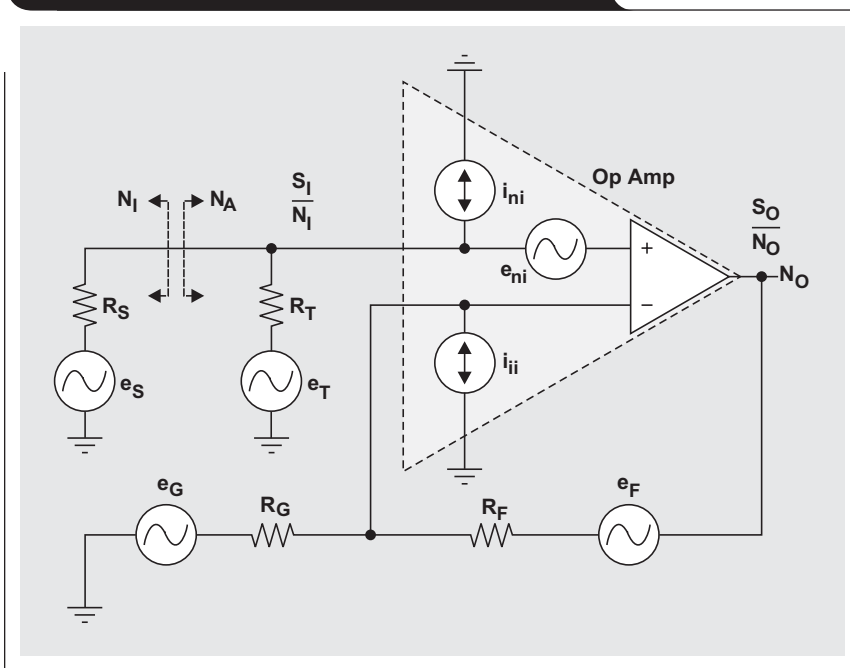
Noise factor of a device is the power ratio of the signal-to-noise ratio (SNR) at the input ( $SNR_I$ ) divided by the SNR at the output ( $SNR_O$ ):

$$F = \frac{SNR_I}{SNR_O} \quad (1)$$

The output signal ( $S_O$ ) is equal to the input signal ( $S_I$ ) times the gain:  $S_O = S_I \times G$ . The output noise is equal to the noise delivered to the input ( $N_I$ ) from the source plus the input noise of the device ( $N_A$ ) times the gain:  $N_O = (N_I + N_A) \times G$ . Substituting into Equation 1 and simplifying, we get

$$F = \frac{SNR_I}{SNR_O} = \left[ \frac{\frac{S_I}{N_I}}{\frac{G \times S_I}{G(N_I + N_A)}} \right] = 1 + \frac{N_A}{N_I} \quad (2)$$

Figure 1. Non-inverting noise analysis diagram



Assuming that the input is terminated in the same impedance as the source,  $N_I = kT = -174 \text{ dBm/Hz}$ , where  $k$  is Boltzman's constant and  $T = 300 \text{ Kelvin}$ ). Once we find the input noise spectral density of the device, it is a simple matter to plug it into Equation 2 and calculate  $F$ .

## NF in op amps

Op amps specify input-referred voltage and current noise. Using these two parameters, adding the noise of the external resistors, and calculating the total input-referred noise based on the circuit topology, we can calculate the input spectral density and use it in Equation 2.

In this discussion, the terms "op amp" and "amplifier" mean different things. "Op amp" refers to only the active device itself, whereas "amplifier" includes the op amp and associated passive resistors that make it work as a usable amplifier stage. In other words, the amplifier is everything shown in Figures 1–3 except  $R_S$ , and the op amp is only the components within the dashed triangles. In this way, the plane marked  $N_A$  and  $N_I$  is the input to the amplifier. This is the point to which the noise sources must be referred so that Equation 2 can be used.

The noise from the source and the input noise of the amplifier are referred to the same point. Because the impedance is the same, expressing the ratio between  $N_A$  and  $N_I$  as a voltage ratio squared is equivalent to the power ratio. An op amp is a voltage-driven device, so using voltage-squared terms makes the calculations easier. In the following discussion, voltage-squared terms are used for  $N_A$  and  $N_I$ .

Op amps use negative feedback to control the gain of the amplifier. One result is that the voltage across the input terminals is driven to zero. This is often referred to as a “virtual short.” It is used in the following analysis\* and referred to as “amplifier action,” since it is a by-product of the op amp doing its job as an amplifier.

Superposition is used throughout the analysis, wherein all sources except the one under consideration are defeated—voltage sources are shorted and current sources are opened.

**Non-inverting amplifier**

Of the three basic op amp circuits, it is easiest to find the input-referred noise for the non-inverting op amp amplifier, so it will be discussed first. Figure 1 shows a noise analysis diagram for a non-inverting op amp amplifier with the noise sources identified.

The source resistance  $R_S$  generates a noise voltage equal to  $\sqrt{4kTR_S}$ . The noise voltage delivered to the amplifier input from the source is divided by the resistors  $R_S$  and  $R_T$ . Therefore,

$$N_I = 4kTR_S \left( \frac{R_T}{R_S + R_T} \right)^2$$

$R_T$  is typically used to terminate the input so that  $R_T = R_S$ , in which case  $N_I = kTR_S$ .

The amplifier’s voltage noise is a combination of  $e_{ni}$ ,  $i_{ni}$ , and  $i_{ii}$  with associated impedances  $e_T$ ,  $e_G$ , and  $e_F$ . These are all referred

**Figure 2. Inverting noise analysis diagram**

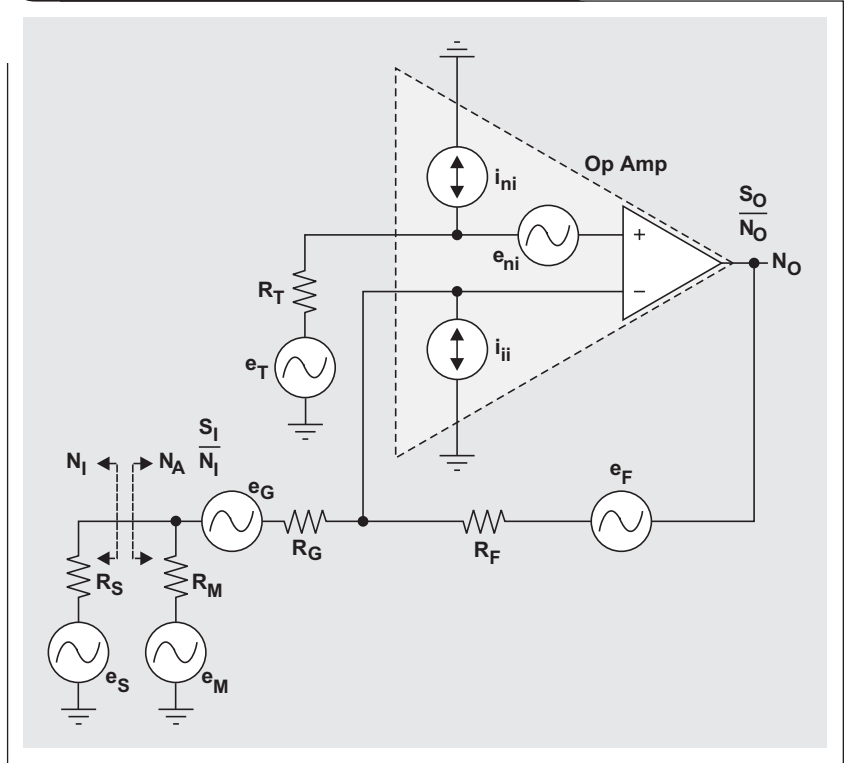
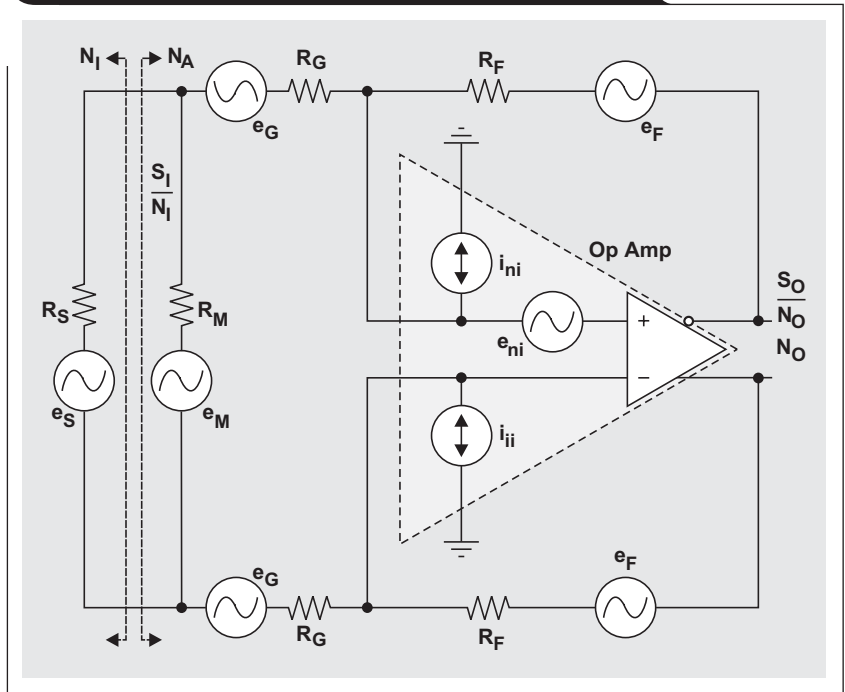


**Figure 3. Fully differential noise analysis diagram**



\*The virtual-short concept simplifies the analysis. Much more work is required to obtain the same results by other means such as nodal analysis.

to the input by their respective scaling factors and summed to find  $N_A$ ; i.e.,

$$N_A = c_1 e_{ni}^2 + c_2 i_{ni}^2 + c_3 i_{ii}^2 + c_4 e_T^2 + c_5 e_G^2 + c_6 e_F^2, \quad (3)$$

where  $c_1$  through  $c_6$  are the scaling factors.

The op amp's input voltage noise is  $e_{ni}$ . It appears directly at the amplifier's input and its scaling factor is 1 or unity, so that  $c_1 e_{ni}^2 = e_{ni}^2$ .

The op amp's non-inverting input current noise is  $i_{ni}$ . It develops a voltage through the parallel combination of  $R_S$  and  $R_T$ , which appears directly at the amplifier's input, so that

$$c_2 i_{ni}^2 = i_{ni}^2 \left( \frac{R_S R_T}{R_S + R_T} \right)^2$$

The op amp's inverting input current noise is  $i_{ii}$ . It develops a voltage through the parallel combination of  $R_F$  and  $R_G$  at the op amp's inverting input. By amplifier action, this voltage appears at the amplifier's input, so that

$$c_3 i_{ii}^2 = i_{ii}^2 \left( \frac{R_F R_G}{R_F + R_G} \right)^2$$

The noise voltage term  $e_T$  associated with  $R_T$  is equal to  $\sqrt{4kTR_T}$ . It is divided by the resistors  $R_S$  and  $R_T$ , so that

$$c_4 e_T^2 = 4kTR_T \left( \frac{R_S}{R_S + R_T} \right)^2$$

If  $R_T = R_S$ , then  $c_4 e_T^2 = kTR_T$ .

The noise voltage term  $e_G$  associated with  $R_G$  is equal to  $\sqrt{4kTR_G}$ . This noise is divided by the resistors  $R_F$  and  $R_G$  and applied to the op amp's inverting input. Again by amplifier action, noise from  $R_G$  appears at the amplifier's input, so that

$$c_5 e_G^2 = 4kTR_G \left( \frac{R_F}{R_F + R_G} \right)^2$$

The noise voltage term  $e_F$  associated with  $R_F$  is equal to  $\sqrt{4kTR_F}$  and appears at the amplifier's output. Dividing by the signal gain gives us

$$c_6 e_F^2 = 4kTR_F \left( \frac{R_G}{R_F + R_G} \right)^2$$

With all the terms in Equation 3 quantified, we can take the sum to find  $N_A$  and use  $N_A$  along with  $N_I$  in Equation 2 to find  $F$ .

### Inverting amplifier

Finding the input-referred noise of an inverting op amp amplifier is more cumbersome than finding that of a non-inverting op amp amplifier. The main problem is that the signal gain of the amplifier and the noise gain are different.

Figure 2 shows a noise analysis diagram for an inverting op amp amplifier with the noise sources identified.

To find the input-referred noise, it is easiest in some cases to find the output noise and then divide by the signal gain of the amplifier.

The noise voltage delivered to the input from the source is divided by the resistors  $R_S$  and  $R_M$  in parallel with  $R_G$ . Therefore,

$$N_I = 4kTR_S \left[ \frac{R_M R_S}{R_S (R_M + R_G) + (R_M R_G)} \right]^2$$

$R_M$  is typically selected so that  $R_M \parallel R_G = R_S$ , in which case  $N_I = kTR_S$ .

The amplifier's input-referred voltage noise is a combination of  $e_{ni}$ ,  $i_{ni}$ , and  $i_{ii}$  with associated impedances  $e_T$ ,  $e_G$ ,  $e_F$ , and  $e_M$ . These are all referred to the input by their respective scaling factors and summed to find  $N_A$ ; i.e.,

$$N_A = c_1 e_{ni}^2 + c_2 i_{ni}^2 + c_3 i_{ii}^2 + c_4 e_T^2 + c_5 e_G^2 + c_6 e_F^2 + c_7 e_M^2, \quad (4)$$

where  $c_1$  through  $c_7$  are the scaling factors.

The op amp's input voltage noise,  $e_{ni}$ , at the op amp's non-inverting input appears at the amplifier output as a function of the amplifier noise gain,

$$1 + \frac{R_F}{R_G + \frac{R_S R_M}{R_S + R_M}}$$

and is then referred back to the amplifier input as a function of the signal gain,  $R_F/R_G$ . Thus,

$$c_1 e_{ni}^2 = e_{ni}^2 \left( \frac{R_G}{R_F} + \frac{R_G}{R_G + \frac{R_S R_M}{R_S + R_M}} \right)^2 **$$

The op amp's non-inverting input current noise is  $i_{ni}$ . It develops a voltage through  $R_T$  that appears directly at the amplifier's input, so that

$$c_2 i_{ni}^2 = i_{ni}^2 \left( \frac{R_T R_G}{R_F} + \frac{R_T R_G}{R_G + \frac{R_S R_M}{R_S + R_M}} \right)^2$$

It is hard to see how to calculate the op amp's inverting input current noise,  $i_{ii}$ . Basically, due to amplifier action, the inverting node is at ground so that no current is drawn through the input resistor  $R_G$ . The noise current flows through  $R_F$ , producing a voltage at the output equal to  $i_{ii} R_F$ . Referring to the amplifier's input results in  $c_3 i_{ii}^2 = i_{ii}^2 (R_G)^2$ .

The noise voltage term  $e_T$  associated with  $R_T$  is equal to  $\sqrt{4kTR_T}$ . Just like  $e_{ni}$ , it appears at the output as a function

\*\*The gain is actually  $-R_F/R_G$ ; but since it is squared, the minus sign is ignored in this analysis.

of the amplifier noise gain and is then referred back to the amplifier input as a function of the signal gain, so that

$$c_4 e_T^2 = kTR_F \left( \frac{R_G}{R_F} + \frac{R_G}{R_G + \frac{R_S R_M}{R_S + R_M}} \right)^2$$

The noise voltage term  $e_G$  associated with  $R_G$  is equal to  $\sqrt{4kTR_G}$ . It is divided by the resistors  $R_G$  and  $R_S$  in parallel with  $R_M$  en route to the amplifier's input, so that

$$c_5 e_G^2 = 4kTR_G \left( \frac{R_G}{R_G + \frac{R_S R_M}{R_S + R_M}} \right)^2$$

The noise voltage term  $e_F$  associated with  $R_F$  is equal to  $\sqrt{4kTR_F}$  and appears directly at the amplifier's output. Dividing by the signal gain gives us

$$c_6 e_F^2 = 4kTR_F \left( \frac{R_G}{R_F} \right)^2$$

The noise source  $e_M$  associated with the input termination matching resistor  $R_M$  is equal to  $\sqrt{4kTR_M}$ . It is divided by the resistors  $R_M$  and  $R_S$  in parallel with  $R_G$ , so that

$$c_7 e_M^2 = 4kTR_M \left[ \frac{R_S R_G}{R_M (R_S + R_G) + R_S R_G} \right]^2$$

With all the terms in Equation 4 quantified, we can take the sum to find  $N_A$  and use  $N_A$  along with  $N_I$  in Equation 2 to find F.

### Fully differential amplifier

Fully differential op amp amplifiers are very similar to inverting op amp amplifiers, and the analysis follows very closely. Figure 3 shows the noise analysis diagram.

The source resistance generates thermal noise equal to  $\sqrt{4kTR_S}$ . The noise voltage delivered to the input from the source is divided by the resistors  $R_S$  and  $R_M$  in parallel with  $2R_G$ . Therefore,

$$N_I = 4kTR_S \left( \frac{\frac{2R_M R_G}{R_M + 2R_G}}{R_S + \frac{2R_M R_G}{R_M + 2R_G}} \right)^2$$

$R_M$  is typically selected so that  $R_M \parallel 2R_G = R_S$ , in which case  $N_I = kTR_S$ .

The amplifier's input-referred voltage noise is a combination of  $e_{ni}$ ,  $i_{ni}$ , and  $i_{ii}$  with associated impedances  $e_G$ ,  $e_F$ , and  $e_M$ . These are all referred to the input by their respective scaling factors and summed to find  $N_A$ ; i.e.,

$$N_A = c_1 e_{ni}^2 + c_2 i_{ni}^2 + c_3 i_{ii}^2 + c_4 e_G^2 + c_5 e_F^2 + c_6 e_M^2 \quad (5)$$

where  $c_1$  through  $c_6$  are the scaling factors.

In this analysis it is assumed that the two input resistors  $R_G$  are equal and that the two feedback resistors  $R_F$  are equal.

The op amp's input voltage noise,  $e_{ni}$ , at the op amp's input appears at the amplifier output as a function of the amplifier noise gain,

$$1 + \frac{R_F}{R_G + \frac{R_S R_M}{2(R_S + R_M)}}$$

and is then referred back to the amplifier input as a function of the signal gain,  $R_F/R_G$ . Thus,

$$c_1 e_{ni}^2 = e_{ni}^2 \left[ \frac{R_G}{R_F} + \frac{R_G}{R_G + \frac{R_S R_M}{2(R_S + R_M)}} \right]^2$$

Since the input resistors are equal and the feedback resistors are equal, the op amp's non-inverting input current noise,  $i_{ni}$ , and inverting input current noise,  $i_{ii}$ , have the same scaling factors. Due to amplifier action, the input nodes of the op amp are ac grounds so that no current is drawn through the input resistors  $R_G$ . All the noise current flows through  $R_F$ , producing a voltage at the output equal to  $i_{ni} R_F$  or  $i_{ii} R_F$ . Referring to the amplifier's input results in  $c_2 i_{ni}^2 = i_{ni}^2 (R_G)^2$  and  $c_3 i_{ii}^2 = i_{ii}^2 (R_G)^2$ .

The noise voltage term  $e_G$  associated with each  $R_G$  is equal to  $\sqrt{4kTR_G}$ . It is divided by the resistors  $R_G$  and one-half  $R_S$  in parallel with  $R_M$ , so that

$$c_4 e_G^2 = 2 \times 4kTR_G \left[ \frac{R_G}{R_G + \frac{R_S R_M}{2(R_S + R_M)}} \right]^2$$

The noise voltage term  $e_F$  associated with each  $R_F$  is equal to  $\sqrt{4kTR_F}$  and appears directly at the amplifier's output. Dividing by the signal gain gives us

$$c_5 e_F^2 = 4kTR_F \left( \frac{R_G}{R_F} \right)^2$$

The noise source  $e_M$  associated with the input termination matching resistor  $R_M$  is equal to  $\sqrt{4kTR_M}$ . It is divided by the resistors  $R_M$  and  $R_S$  in parallel with  $2R_G$ , so that

$$c_6 e_M^2 = 4kTR_M \left( \frac{\frac{2R_S R_G}{R_S + 2R_G}}{R_M + \frac{2R_S R_G}{R_S + 2R_G}} \right)^2$$

As before, with all the terms in Equation 5 quantified,  $N_A$  can be calculated and used with  $N_I$  in Equation 2 to find the noise factor.

**Table 1. Comparison of calculated vs. measured noise figure**

OP AMP	CONFIGURATION	$e_{ni}$ (nV)	$i_{ni}$ (pA)	$i_{ii}$ (pA)	$R_F$ ( $\Omega$ )	$R_G$ ( $\Omega$ )	$R_T$ ( $\Omega$ )	$R_M$ ( $\Omega$ )	CALCULATED NF (dB)	MEASURED NF (dB)
THS3202	Non-inverting	1.65	13.5	20	255	49.9	49.9	—	11.6	11.5
THS3202	Inverting	1.65	13.5	20	255	49.9	—	—	13.6	13.0
THS4501	Fully differential	7	1.7	1.7	392	392	—	56.2	30.1	30.6

## Conclusion

The input-referred voltage noise and current noise, along with the circuit configuration and component values, can be used to calculate noise figure. This is a tedious task at best. Setting up a spreadsheet for each topology where component values and op amp specs can be entered is recommended. In this way, various scenarios can be quickly tested. Verification by testing the circuit with a noise figure analyzer is always suggested.

As an example of how well the theory outlined in this article matches test results, the noise figure of three op amp

amplifiers configured as previously detailed were measured with an Agilent N8973A noise figure analyzer. Table 1 shows that the results are good, with the input current and voltage noise specifications given as typical values.

## Related Web sites

[analog.ti.com](http://analog.ti.com)

[www.ti.com/sc/device/THS3202](http://www.ti.com/sc/device/THS3202)

[www.ti.com/sc/device/THS4501](http://www.ti.com/sc/device/THS4501)

## Appendix—Summary of noise terms in op amp amplifiers

### Signal input noise ( $N_I$ ) terms

AMPLIFIER CONFIGURATION	NOISE SOURCE	NOISE CONTRIBUTION
Non-inverting	Source thermal noise	$4kTR_S \left( \frac{R_T}{R_S + R_T} \right)^2$
Inverting	Source thermal noise	$N_I = 4kTR_S \left[ \frac{R_M R_S}{R_S (R_M + R_G) + (R_M R_G)} \right]^2$
Fully differential	Source thermal noise	$4kTR_S \left( \frac{\frac{2R_M R_G}{R_M + 2R_G}}{R_S + \frac{2R_M R_G}{R_M + 2R_G}} \right)^2$

## Appendix—Summary of noise terms in op amp amplifiers (Continued)

### Device input noise ( $N_A$ ) terms

AMPLIFIER CONFIGURATION	NOISE SOURCE	NOISE CONTRIBUTION
Non-inverting	Op amp input-referred voltage noise	$e_{ni}^2$
	Op amp non-inverting input-referred current noise	$i_{ni}^2 \left( \frac{R_S R_T}{R_S + R_T} \right)^2$
	Op amp inverting input-referred current noise	$i_{ii}^2 \left( \frac{R_F R_G}{R_F + R_G} \right)^2$
	Termination resistor thermal noise voltage	$4kTR_T \left( \frac{R_S}{R_S + R_T} \right)^2$
	Gain resistor thermal noise voltage	$4kTR_G \left( \frac{R_F}{R_F + R_G} \right)^2$
	Feedback resistor thermal noise voltage	$4kTR_F \left( \frac{R_G}{R_F + R_G} \right)^2$
Inverting	Op amp input-referred voltage noise	$e_{ni}^2 \left( \frac{R_G}{R_F} + \frac{R_G}{R_G + \frac{R_S R_M}{R_S + R_M}} \right)^2$
	Op amp non-inverting input-referred current noise	$i_{ni}^2 \left( \frac{R_T R_G}{R_F} + \frac{R_T R_G}{R_G + \frac{R_S R_M}{R_S + R_M}} \right)^2$
	Op amp inverting input-referred current noise	$i_{ii}^2 (R_G)^2$
	Non-inverting bias matching resistor thermal noise voltage	$4kTR_T \left( \frac{R_G}{R_F} + \frac{R_G}{R_G + \frac{R_S R_M}{R_S + R_M}} \right)^2$
	Gain resistor thermal noise voltage	$4kTR_G \left( \frac{R_G}{R_G + \frac{R_S R_M}{R_S + R_M}} \right)^2$
	Feedback resistor thermal noise voltage	$4kTR_F \left( \frac{R_G}{R_F} \right)^2$
	Inverting termination matching resistor thermal noise voltage	$4kTR_M \left[ \frac{R_S R_G}{R_M (R_S + R_G) + R_S R_G} \right]^2$

## Appendix—Summary of noise terms in op amp amplifiers (Continued)

### Device input noise ( $N_A$ ) terms (Continued)

AMPLIFIER CONFIGURATION	NOISE SOURCE	NOISE CONTRIBUTION
Fully differential	Op amp input-referred voltage noise	$e_{ni}^2 \left[ \frac{R_G}{R_F} + \frac{R_G}{R_G + \frac{R_S R_M}{2(R_S + R_M)}} \right]^2$
	Op amp non-inverting input-referred current noise	$i_{ni}^2 (R_G)^2$
	Op amp inverting input-referred current noise	$i_{ii}^2 (R_G)^2$
	Gain resistor thermal noise voltage	$2 \times 4kTR_G \left[ \frac{R_G}{R_G + \frac{R_S R_M}{2(R_S + R_M)}} \right]^2$
	Feedback resistor thermal noise voltage	$2 \times 4kTR_F \left( \frac{R_G}{R_F} \right)^2$
	Termination matching resistor thermal noise voltage	$4kTR_M \left( \frac{\frac{2R_S R_G}{R_S + 2R_G}}{R_M + \frac{2R_S R_G}{R_S + 2R_G}} \right)^2$

# Index of Articles

Title	Issue	Page
<b>Data Acquisition</b>		
Aspects of data acquisition system design	August 1999	1
Low-power data acquisition sub-system using the TI TLV1572	August 1999	4
Evaluating operational amplifiers as input amplifiers for A-to-D converters	August 1999	7
Precision voltage references	November 1999	1
Techniques for sampling high-speed graphics with lower-speed A/D converters	November 1999	5
A methodology of interfacing serial A-to-D converters to DSPs	February 2000	1
The operation of the SAR-ADC based on charge redistribution	February 2000	10
The design and performance of a precision voltage reference circuit for 14-bit and 16-bit A-to-D and D-to-A converters	May 2000	1
Introduction to phase-locked loop system modeling	May 2000	5
New DSP development environment includes data converter plug-ins (PDF - 86 Kb)	August 2000	1
Higher data throughput for DSP analog-to-digital converters (PDF - 94 Kb)	August 2000	5
Efficiently interfacing serial data converters to high-speed DSPs (PDF - 80 Kb)	August 2000	10
Smallest DSP-compatible ADC provides simplest DSP interface (PDF - 120 Kb)	November 2000	1
Hardware auto-identification and software auto-configuration for the TLV320AIC10 DSP Codec — a “plug-and-play” algorithm (PDF - 105 Kb)	November 2000	8
Using quad and octal ADCs in SPI mode (PDF - 94 Kb)	November 2000	15
Building a simple data acquisition system using the TMS320C31 DSP (PDF - 235 Kb)	February 2001	1
Using SPI synchronous communication with data converters — interfacing the MSP430F149 and TLV5616 (PDF - 182 Kb)	February 2001	7
A/D and D/A conversion of PC graphics and component video signals, Part 1: Hardware (PDF - 191 Kb)	February 2001	11
A/D and D/A conversion of PC graphics and component video signals, Part 2: Software and control	July 2001	5
Intelligent sensor system maximizes battery life: Interfacing the MSP430F123 Flash MCU, ADS7822, and TPS60311	First Quarter, 2002	5
SHDSL AFE1230 application	Second Quarter, 2002	5
Synchronizing non-FIFO variations of the THS1206	Second Quarter, 2002	12
Adjusting the A/D voltage reference to provide gain	Third Quarter, 2002	5
MSC1210 debugging strategies for high-precision smart sensors	Third Quarter, 2002	7
Using direct data transfer to maximize data acquisition throughput	Third Quarter, 2002	14
Interfacing op amps and analog-to-digital converters	Fourth Quarter, 2002	5
ADS82x ADC with non-uniform sampling clock	Fourth Quarter, 2003	5
Calculating noise figure and third-order intercept in ADCs	Fourth Quarter, 2003	11
Evaluation criteria for ADSL analog front end	Fourth Quarter, 2003	16
<b>Power Management</b>		
Stability analysis of low-dropout linear regulators with a PMOS pass element	August 1999	10
Extended output voltage adjustment (0 V to 3.5 V) using the TI TPS5210	August 1999	13
Migrating from the TI TL770x to the TI TLC770x	August 1999	14
TI TPS5602 for powering TI's DSP	November 1999	8
Synchronous buck regulator design using the TI TPS5211 high-frequency hysteretic controller	November 1999	10
Understanding the stable range of equivalent series resistance of an LDO regulator	November 1999	14
Power supply solutions for TI DSPs using synchronous buck converters	February 2000	12
Powering Celeron-type microprocessors using TI's TPS5210 and TPS5211 controllers	February 2000	20
Simple design of an ultra-low-ripple DC/DC boost converter with TPS60100 charge pump	May 2000	11
Low-cost, minimum-size solution for powering future-generation Celeron™-type processors with peak currents up to 26 A	May 2000	14

Title	Issue	Page
<b>Power Management (Continued)</b>		
Advantages of using PMOS-type low-dropout linear regulators in battery applications (PDF - 216 Kb)	August 2000	16
Optimal output filter design for microprocessor or DSP power supply (PDF - 748 Kb)	August 2000	22
Understanding the load-transient response of LDOs (PDF - 241 Kb)	November 2000	19
Comparison of different power supplies for portable DSP solutions working from a single-cell battery (PDF - 136 Kb)	November 2000	24
Optimal design for an interleaved synchronous buck converter under high-slew-rate, load-current transient conditions (PDF - 206 Kb)	February 2001	15
-48-V/+48-V hot-swap applications (PDF - 189 Kb)	February 2001	20
Power supply solution for DDR bus termination	July 2001	9
Runtime power control for DSPs using the TPS62000 buck converter	July 2001	15
Power control design key to realizing InfiniBand <sup>SM</sup> benefits	First Quarter, 2002	10
Comparing magnetic and piezoelectric transformer approaches in CCFL applications	First Quarter, 2002	12
Why use a wall adapter for ac input power?	First Quarter, 2002	18
SWIFT <sup>TM</sup> Designer power supply design program	Second Quarter, 2002	15
Optimizing the switching frequency of ADSL power supplies	Second Quarter, 2002	23
Powering electronics from the USB port	Second Quarter, 2002	28
Using the UCC3580-1 controller for highly efficient 3.3-V/100-W isolated supply design	Fourth Quarter, 2002	8
Power conservation options with dynamic voltage scaling in portable DSP designs	Fourth Quarter, 2002	12
Understanding piezoelectric transformers in CCFL backlight applications	Fourth Quarter, 2002	18
Load-sharing techniques: Paralleling power modules with overcurrent protection	First Quarter, 2003	5
Using the TPS61042 white-light LED driver as a boost converter	First Quarter, 2003	7
Auto-Track <sup>TM</sup> voltage sequencing simplifies simultaneous power-up and power-down	Third Quarter, 2003	5
Soft-start circuits for LDO linear regulators	Third Quarter, 2003	10
UCC28517 100-W PFC power converter with 12-V, 8-W bias supply, Part 1	Third Quarter, 2003	13
UCC28517 100-W PFC power converter with 12-V, 8-W bias supply, Part 2	Fourth Quarter, 2003	21
<b>Interface (Data Transmission)</b>		
TIA/EIA-568A Category 5 cables in low-voltage differential signaling (LVDS)	August 1999	16
Keep an eye on the LVDS input levels	November 1999	17
Skew definition and jitter analysis	February 2000	29
LVDS receivers solve problems in non-LVDS applications	February 2000	33
LVDS: The ribbon cable connection	May 2000	19
Performance of LVDS with different cables (PDF - 57 Kb)	August 2000	30
A statistical survey of common-mode noise (PDF - 131 Kb)	November 2000	30
The Active Fail-Safe feature of the SN65LVDS32A (PDF - 104 Kb)	November 2000	35
The SN65LVDS33/34 as an ECL-to-LVTTL converter	July 2001	19
Power consumption of LVPECL and LVDS	First Quarter, 2002	23
<b>Amplifiers: Audio</b>		
Reducing the output filter of a Class-D amplifier	August 1999	19
Power supply decoupling and audio signal filtering for the Class-D audio power amplifier	August 1999	24
PCB layout for the TPA005D1x and TPA032D0x Class-D APAs	February 2000	39
An audio circuit collection, Part 1 (PDF - 93 Kb)	November 2000	39
1.6- to 3.6-volt BTL speaker driver reference design (PDF - 194 Kb)	February 2001	23
Notebook computer upgrade path for audio power amplifiers (PDF - 202 Kb)	February 2001	27
An audio circuit collection, Part 2 (PDF - 215 Kb)	February 2001	41
An audio circuit collection, Part 3	July 2001	34
Audio power amplifier measurements	July 2001	40
Audio power amplifier measurements, Part 2	First Quarter, 2002	26

Title	Issue	Page
<b>Amplifiers: Op Amps</b>		
Single-supply op amp design .....	November 1999 .....	20
Reducing crosstalk of an op amp on a PCB .....	November 1999 .....	23
Matching operational amplifier bandwidth with applications .....	February 2000 .....	36
Sensor to ADC — analog interface design .....	May 2000 .....	22
Using a decompensated op amp for improved performance .....	May 2000 .....	26
Design of op amp sine wave oscillators (PDF - 56 Kb) .....	August 2000 .....	33
Fully differential amplifiers (PDF - 51 Kb) .....	August 2000 .....	38
The PCB is a component of op amp design (PDF - 64 Kb) .....	August 2000 .....	42
Reducing PCB design costs: From schematic capture to PCB layout (PDF - 28 Kb) .....	August 2000 .....	48
Thermistor temperature transducer-to-ADC application (PDF - 97 Kb) .....	November 2000 .....	44
Analysis of fully differential amplifiers (PDF - 96 Kb) .....	November 2000 .....	48
Fully differential amplifiers applications: Line termination, driving high-speed ADCs, and differential transmission lines (PDF - 185 Kb) .....	February 2001 .....	32
Pressure transducer-to-ADC application (PDF - 185 Kb) .....	February 2001 .....	38
Frequency response errors in voltage feedback op amps (PDF - 184 Kb) .....	February 2001 .....	48
Designing for low distortion with high-speed op amps .....	July 2001 .....	25
Fully differential amplifier design in high-speed data acquisition systems .....	Second Quarter, 2002 ..	35
Worst-case design of op amp circuits .....	Second Quarter, 2002 ..	42
Using high-speed op amps for high-performance RF design, Part 1 .....	Second Quarter, 2002 ..	46
Using high-speed op amps for high-performance RF design, Part 2 .....	Third Quarter, 2002 ..	21
FilterPro™ low-pass design tool .....	Third Quarter, 2002 ..	24
Active output impedance for ADSL line drivers .....	Fourth Quarter, 2002 ..	24
RF and IF amplifiers with op amps .....	First Quarter, 2003 .....	9
Analyzing feedback loops containing secondary amplifiers .....	First Quarter, 2003 .....	14
Video switcher using high-speed op amps .....	Third Quarter, 2003 ..	20
Expanding the usability of current-feedback amplifiers .....	Third Quarter, 2003 ..	23
Calculating noise figure in op amps .....	Fourth Quarter, 2003 ..	28
<b>General Interest</b>		
Synthesis and characterization of nickel manganite from different carboxylate precursors for thermistor sensors (PDF - 194 Kb) .....	February 2001 .....	52
Analog design tools .....	Second Quarter, 2002 ..	50

## TI Worldwide Technical Support

### Internet

#### TI Semiconductor Product Information Center Home Page

support.ti.com

#### TI Semiconductor KnowledgeBase Home Page

support.ti.com/sc/knowledgebase

### Product Information Centers

#### Americas

Phone +1(972) 644-5580  
 Fax +1(972) 927-6377  
 Internet/Email support.ti.com/sc/pic/americas.htm

#### Europe, Middle East, and Africa

Phone  
 Belgium (English) +32 (0) 27 45 55 32  
 Finland (English) +358 (0) 9 25173948  
 France +33 (0) 1 30 70 11 64  
 Germany +49 (0) 8161 80 33 11  
 Israel (English) 1800 949 0107  
 Italy 800 79 11 37  
 Netherlands (English) +31 (0) 546 87 95 45  
 Spain +34 902 35 40 28  
 Sweden (English) +46 (0) 8587 555 22  
 United Kingdom +44 (0) 1604 66 33 99  
 Fax +(49) (0) 8161 80 2045  
 Email epic@ti.com  
 Internet support.ti.com/sc/pic/euro.htm

#### Japan

Fax International +81-3-3344-5317  
 Domestic 0120-81-0036  
 Internet/Email International support.ti.com/sc/pic/japan.htm  
 Domestic www.tij.co.jp/pic

#### Asia

Phone  
 International +886-2-23786800  
 Domestic Toll-Free Number  
 Australia 1-800-999-084  
 China 108-00-886-0015  
 Hong Kong 800-96-5941  
 Indonesia 001-803-8861-1006  
 Korea 080-551-2804  
 Malaysia 1-800-80-3973  
 New Zealand 0800-446-934  
 Philippines 1-800-765-7404  
 Singapore 800-886-1028  
 Taiwan 0800-006800  
 Thailand 001-800-886-0010  
 Fax 886-2-2378-6808  
 Email tiasia@ti.com  
 Internet support.ti.com/sc/pic/asia.htm

**Important Notice:** The products and services of Texas Instruments Incorporated and its subsidiaries described herein are sold subject to TI's standard terms and conditions of sale. Customers are advised to obtain the most current and complete information about TI products and services before placing orders. TI assumes no liability for applications assistance, customer's applications or product designs, software performance, or infringement of patents. The publication of information regarding any other company's products or services does not constitute TI's approval, warranty or endorsement thereof.

A010203

Auto-Track Sequencing, CommsADC, FilterPro and SWIFT are trademarks of Texas Instruments. Celeron is a trademark of Intel Corporation. InfiniBand is a registered trademark and service mark of the InfiniBand Trade Association.

SLYT051A

38

## IMPORTANT NOTICE

Texas Instruments Incorporated and its subsidiaries (TI) reserve the right to make corrections, enhancements, improvements and other changes to its semiconductor products and services per JESD46, latest issue, and to discontinue any product or service per JESD48, latest issue. Buyers should obtain the latest relevant information before placing orders and should verify that such information is current and complete. All semiconductor products (also referred to herein as "components") are sold subject to TI's terms and conditions of sale supplied at the time of order acknowledgment.

TI warrants performance of its components to the specifications applicable at the time of sale, in accordance with the warranty in TI's terms and conditions of sale of semiconductor products. Testing and other quality control techniques are used to the extent TI deems necessary to support this warranty. Except where mandated by applicable law, testing of all parameters of each component is not necessarily performed.

TI assumes no liability for applications assistance or the design of Buyers' products. Buyers are responsible for their products and applications using TI components. To minimize the risks associated with Buyers' products and applications, Buyers should provide adequate design and operating safeguards.

TI does not warrant or represent that any license, either express or implied, is granted under any patent right, copyright, mask work right, or other intellectual property right relating to any combination, machine, or process in which TI components or services are used. Information published by TI regarding third-party products or services does not constitute a license to use such products or services or a warranty or endorsement thereof. Use of such information may require a license from a third party under the patents or other intellectual property of the third party, or a license from TI under the patents or other intellectual property of TI.

Reproduction of significant portions of TI information in TI data books or data sheets is permissible only if reproduction is without alteration and is accompanied by all associated warranties, conditions, limitations, and notices. TI is not responsible or liable for such altered documentation. Information of third parties may be subject to additional restrictions.

Resale of TI components or services with statements different from or beyond the parameters stated by TI for that component or service voids all express and any implied warranties for the associated TI component or service and is an unfair and deceptive business practice. TI is not responsible or liable for any such statements.

Buyer acknowledges and agrees that it is solely responsible for compliance with all legal, regulatory and safety-related requirements concerning its products, and any use of TI components in its applications, notwithstanding any applications-related information or support that may be provided by TI. Buyer represents and agrees that it has all the necessary expertise to create and implement safeguards which anticipate dangerous consequences of failures, monitor failures and their consequences, lessen the likelihood of failures that might cause harm and take appropriate remedial actions. Buyer will fully indemnify TI and its representatives against any damages arising out of the use of any TI components in safety-critical applications.

In some cases, TI components may be promoted specifically to facilitate safety-related applications. With such components, TI's goal is to help enable customers to design and create their own end-product solutions that meet applicable functional safety standards and requirements. Nonetheless, such components are subject to these terms.

No TI components are authorized for use in FDA Class III (or similar life-critical medical equipment) unless authorized officers of the parties have executed a special agreement specifically governing such use.

Only those TI components which TI has specifically designated as military grade or "enhanced plastic" are designed and intended for use in military/aerospace applications or environments. Buyer acknowledges and agrees that any military or aerospace use of TI components which have **not** been so designated is solely at the Buyer's risk, and that Buyer is solely responsible for compliance with all legal and regulatory requirements in connection with such use.

TI has specifically designated certain components as meeting ISO/TS16949 requirements, mainly for automotive use. In any case of use of non-designated products, TI will not be responsible for any failure to meet ISO/TS16949.

### Products

Audio	<a href="http://www.ti.com/audio">www.ti.com/audio</a>
Amplifiers	<a href="http://amplifier.ti.com">amplifier.ti.com</a>
Data Converters	<a href="http://dataconverter.ti.com">dataconverter.ti.com</a>
DLP® Products	<a href="http://www.dlp.com">www.dlp.com</a>
DSP	<a href="http://dsp.ti.com">dsp.ti.com</a>
Clocks and Timers	<a href="http://www.ti.com/clocks">www.ti.com/clocks</a>
Interface	<a href="http://interface.ti.com">interface.ti.com</a>
Logic	<a href="http://logic.ti.com">logic.ti.com</a>
Power Mgmt	<a href="http://power.ti.com">power.ti.com</a>
Microcontrollers	<a href="http://microcontroller.ti.com">microcontroller.ti.com</a>
RFID	<a href="http://www.ti-rfid.com">www.ti-rfid.com</a>
OMAP Applications Processors	<a href="http://www.ti.com/omap">www.ti.com/omap</a>
Wireless Connectivity	<a href="http://www.ti.com/wirelessconnectivity">www.ti.com/wirelessconnectivity</a>

### Applications

Automotive and Transportation	<a href="http://www.ti.com/automotive">www.ti.com/automotive</a>
Communications and Telecom	<a href="http://www.ti.com/communications">www.ti.com/communications</a>
Computers and Peripherals	<a href="http://www.ti.com/computers">www.ti.com/computers</a>
Consumer Electronics	<a href="http://www.ti.com/consumer-apps">www.ti.com/consumer-apps</a>
Energy and Lighting	<a href="http://www.ti.com/energy">www.ti.com/energy</a>
Industrial	<a href="http://www.ti.com/industrial">www.ti.com/industrial</a>
Medical	<a href="http://www.ti.com/medical">www.ti.com/medical</a>
Security	<a href="http://www.ti.com/security">www.ti.com/security</a>
Space, Avionics and Defense	<a href="http://www.ti.com/space-avionics-defense">www.ti.com/space-avionics-defense</a>
Video and Imaging	<a href="http://www.ti.com/video">www.ti.com/video</a>

### TI E2E Community

[e2e.ti.com](http://e2e.ti.com)